Evolutionary population synthesis: models, analysis of the ingredients and application to high-z galaxies

Claudia Maraston*†

Max-Planck-Institut für extraterrestrische Physik, Giessenbachstraße, D-85748 Garching b. München, Germany

ABSTRACT

Evolutionary population synthesis models for a wide range of metallicities, ages, star formation histories, initial mass functions and horizontal branch morphologies, including blue morphologies at high metallicity, are computed. The model output comprises spectral energy distributions, colours, stellar M/L ratios, bolometric corrections and near-infrared (IR) spectral line indices. The energetics of the post main sequence evolutionary phases are evaluated with the fuel consumption theorem. The impact on the models of the stellar evolutionary tracks (in particular with and without overshooting) is assessed. We find modest differences in synthetic broad-band colours as induced by the use of different tracks in our code [e.g. $\Delta(V - K) \sim 0.08$ mag, $\Delta(B - V) \sim 0.03$ mag]. Noticeably, these differences are substantially smaller than the scatter among other models in the literature, even when the latter adopt the same evolutionary tracks. The models are calibrated with globular cluster data from the Milky Way for old ages, and the Magellanic clouds plus the merger remnant galaxy NGC 7252, both for young ages of $\sim$0.1–2 Gyr, in a large wavelength range from the U band to the K band. Particular emphasis is put on the contribution from the thermally pulsing asymptotic giant branch (TP-AGB) phase. We show that this evolutionary phase is crucial for the modelling of young stellar populations by direct comparison with observed spectral energy distributions of Magellanic cloud clusters, which are characterized by relatively high fluxes, both blueward and redward of the V band. We find that the combination of the near-IR spectral indices C_2 and H_2O can be used to determine the metallicity of $\sim$1 Gyr stellar populations. As an illustrative application, we re-analyse the spectral energy distributions of some of the high-z galaxies ($2.4 \lesssim z \lesssim 2.9$) observed with the *Spitzer Space Telescope* by Yan et al. Their high rest-frame near-IR fluxes is reproduced very well with the models including TP-AGB stars for ages in the range $\sim$0.6–1.5 Gyr, suggesting formation redshifts for these objects around $z \sim 3$–6.

Key words: stars: AGB and post-AGB – stars: evolution – galaxies: evolution – galaxies: stellar content – cosmology: early Universe.

1 INTRODUCTION

The evolutionary population synthesis (EPS) is the technique to model the spectrophotometric properties of stellar populations, which uses the knowledge of stellar evolution. This approach was pioneered by Tinsley in a series of fundamental papers that provide the basic concepts still used in present-day computations. The models are used to determine ages, element abundances, stellar masses, stellar mass functions, etc., of those stellar populations that are not resolvable in single stars, like galaxies and extragalactic globular clusters (GCs). Due to the ubiquitous astrophysical applications of

EPS models, a rich literature has been developed so far (Bruzual 1983; Renzini & Buzzoni 1986; Chiosi, Bertelli & Bressan 1988; Buzzoni 1989; Charlot & Bruzual 1991; Bruzual & Charlot 1993; Worthey 1994; Tantalo et al. 1996; Vazdekis et al. 1996; Fioc & Rocca-Volmerange 1997; Bressan, Granato & Silva 1998; Maraston 1998; Leitherer et al. 1999; Brocato et al. 2000; Thomas, Maraston & Bender 2003a; Thomas, Maraston & Korn 2004).

In the simplest flavour of an EPS model, called *simple stellar population* (hereafter SSP) by Renzini (1981), it is assumed that all stars are coeval and share the same chemical composition. The advantage of dealing with SSPs is twofold. First, SSPs can be compared directly with GC data, since these are the 'simplest' stellar populations in nature. This offers the advantage of *calibrating* the SSPs with those GCs for which ages and element abundances are independently known, an approach introduced in the review by Renzini & Fusi Pecci (1988). This step is crucial to fix the

*Present address: University of Oxford, Denys Wilkinson Building, Keble Road, Oxford, OX1 3RH, UK.
†E-mail: maraston@astro.ox.ac.uk

parameters that are used to describe that part of the model 'input physics' – convection, mass loss and mixing – which cannot be derived from first principles. The calibrated models can be applied with more confidence to the study of extragalactic stellar populations. This step is taken in the models of Maraston (1998) and in their extension presented here. Secondly, complex stellar systems that are made up by various stellar generations are modelled by convolving SSPs with the adopted star formation history (e.g. Tinsley 1972; Arimoto & Yoshii 1986; Rocca-Volmerange & Guiderdoni 1987; Vazdekis et al. 1996; Barbaro & Poggianti 1997; Kodama & Arimoto 1997; Bruzual & Charlot 2003). Therefore, the deep knowledge of the building blocks of complex models is very important.

Two techniques are adopted to compute SSP models, which differ according to the integration variable adopted in the post main sequence (PMS): isochrone synthesis and 'fuel-consumption-based' algorithms. With the 'isochrone synthesis' (e.g. Chiosi et al. 1988; Charlot & Bruzual 1991) the properties of a stellar population are calculated by integrating the contributions to the flux in the various passbands of all mass bins along one isochrone, after assuming an initial mass function (IMF). Usually, isochrones are computed up to the end of the early asymptotic giant branch (E-AGB) phase. Later stellar phases like the thermally pulsing asymptotic giant branch (TP-AGB) are added following individual recipes or are neglected.

In the 'fuel consumption' approach (Renzini 1981; Renzini & Buzzoni 1986; Buzzoni 1989; Maraston 1998), the integration variable in PMS is the so-called *fuel*, that is, the amount of hydrogen and/or helium that is consumed via nuclear burning during a given PMS phase. The fuel at a given age is computed on the stellar evolutionary track of the *turnoff* mass (i.e. the mass completing the hydrogen-burning phase), thereby neglecting the dispersion of stellar masses in PMS. However, since a mass difference of only few per cent exists between the *turnoff* mass and the mass at any other PMS phase, this assumption can be made safely, as also shown by Charlot & Bruzual (1991). The advantages of the fuel consumption approach are of two kinds. First, the fuel as integration variable is very stable since it is directly proportional to the contributions of the various phases to the total luminosity. This is very important in luminous, but short-lived evolutionary stages, e.g. the bright red giant branch (RGB) phase, where the evolutionary mass practically does not change. We note that the problem of the numerical instability on the RGB was early recognized by Tinsley & Gunn (1976). Secondly, and more importantly, there are several relevant stellar phases [e.g. blue horizontal branch (BHB), TP-AGB, very hot old stars, etc.] whose theoretical modelling is uncertain because of mass loss and for which complete stellar tracks are not available. The fuel consumption provides useful analytical relations that link the main sequence (MS) to the PMS evolution, by means of which one can include into the synthesis the energy contributions of these uncertain phases using, for example, observations. The 'isochrone synthesis' technique is used in all models in the literature, with the exception of the models by Buzzoni (1989), Maraston (1998) and those presented here, which adopt the fuel consumption theorem.

Besides the method used to compute them, EPS models keep the uncertainties inherent in the stellar evolutionary tracks and in the spectral transformations. Charlot, Worthey & Bressan (1996) investigated both classes of uncertainties by comparing their EPS models. The analysis is very illustrative for the three considered EPS; however, it does not yield information about the sole impact of the stellar tracks. Here we make a different exercise, because we can use the same EPS code and just vary the model ingredients. In this way, we can isolate their impact on the final model. Quantifying the model uncertainties is indeed very important since the cosmological inferences that are derived on the basis of galaxy ages and metallicities rely ultimately on the stellar population models.

Maraston (1998) presents a fuel-consumption-based code for EPS, SSP models for solar metallicity and ages from 30 Myr to 15 Gyr. Distinct features of that work are

(i) the extension of the fuel consumption theorem to compute models for young and intermediate-range ages;

(ii) the inclusion of a well-calibrated semi-empirical TP-AGB phase, and the computation of realistic colours of intermediate-age ($t \lesssim 2$ Gyr) stellar populations;

(iii) the modular structure of the code that allows experiments with the EPS ingredients.

Subsequently, the code has been updated to the computations of SSP models covering a wide range in metallicities, and the model output has been extended to, e.g., the spectral energy distributions (SEDs), spectral indices and redshift evolution, with several applications being already published (Maraston & Thomas 2000; Saglia et al. 2000; Maraston et al. 2001a, 2003; Thomas et al. 2003a, 2004a; Ferraro et al. 2004). This work is devoted to discussing comprehensively the overall EPS models and ingredients, in particular, the inclusion of the TP-AGB phase in the synthetic SEDs.

The paper is organized as follows. In Section 2, the properties of the EPS code are recalled. The model ingredients, i.e. the fuel consumptions, the temperature distributions and the model atmospheres, for the various metallicities and ages, are described in detail in Section 3. In particular, the recipes for horizontal branch (HB) and TP-AGB are presented in Section 3.4. The various model output are discussed in Section 4, where the comparisons with observational data and with models from the literatures are also presented. Section 5 deals with the model uncertainties, while Section 6 presents a high-redshift application of the model SEDs in which the TP-AGB has a primary importance. Finally, a summary of the main results is given in Section 7.

2 ALGORITHM

In this section, we recall the basic equations that define the algorithm of the EPS code by Maraston (1998, hereafter M98). Following Renzini & Buzzoni (1986, hereafter RB86), the total bolometric luminosity of a SSP of age t and chemical composition $[Y, Z]$ is split conveniently into the contributions by MS and PMS as

$$L_{\mathrm{SSP}}^{\mathrm{bol}}(t; [Y, Z]) = L_{\mathrm{MS}}^{\mathrm{bol}}(t; [Y, Z]) + L_{\mathrm{PMS}}^{\mathrm{bol}}(t; [Y, Z]), \qquad (1)$$

because the two quantities depend on different ingredients. The MS light is produced by stars spanning a very wide mass range, while the PMS one is produced by stars of virtually the same mass. Therefore, $L_{\mathrm{MS}}^{\mathrm{bol}}$ depends on the adopted mass–luminosity relation $L(M, t)$ and IMF, $\Psi(M) = AM^{-s}$ (A being the scalefactor related to the size of the stellar population), while $L_{\mathrm{PMS}}^{\mathrm{bol}}$ depends on the nuclear fuel burned in the various evolved stellar stages. The MS luminosities are computed by integrating the contributions by each mass bin along an isochrone, from a lower mass limit M_{inf} (usually 0.1 $\mathrm{M_\odot}$) to the current turnoff mass $M_{\mathrm{TO}}(t)$, having assumed an IMF $\Psi(M)$

$$L_{\mathrm{MS}}^{\mathrm{bol}}(t; [Y, Z]) = \int_{M_{\mathrm{inf}}}^{M_{\mathrm{TO}}} L(\mathrm{M}(t; [Y, Z])) \psi(\mathrm{M}) \, \mathrm{d}M. \qquad (2)$$

The PMS luminosity contributions are computed by means of the *fuel consumption theorem* (RB86)

$$L_{\mathrm{PMS}}^{\mathrm{bol}}(t; [Y, Z]) = 9.75 \times 10^{10} b(t) \sum_J \mathrm{Fuel}_J[M_{\mathrm{TO}}(t; [Y, Z])], \quad (3)$$

where the *evolutionary flux*

$$b(t; [Y, Z]) = \psi[M_{\mathrm{TO}}(t; [Y, Z])]|\dot{M}_{\mathrm{TO}}| \quad (4)$$

provides the rate of stars evolving to any PMS phase j at the age t of the stellar population, and $\mathrm{Fuel}_J[M_{\mathrm{TO}}(t; Y, Z)]$ is the amount of stellar mass to be converted in luminosity in each of these phases. The multiplicative factor in equation (3) stems from expressing the luminosity in solar units, the evolutionary flux $b(t)$ in years and the fuel in solar masses through the Einstein equation $E = \Delta M c^2$, with $\Delta = 6.55 \times 10^{-3}$. The latter is derived by considering that the transformation of 1 g of H into He releases $\sim 5.9 \times 10^{18}$ erg. This average value takes into account the dependence on whether the carbon–nitrogen–oxygen cycle or the pp chain is at work and the different neutrino losses as a function of the temperature of the burning (Renzini 1981).

3 INGREDIENTS

Following M98, the ingredients of evolutionary synthesis models are as follows.

(i) *The energetics*: mass–luminosity relations for the MS and fuel consumptions for PMS phases.

(ii) *The surface parameters*: the effective temperatures and surface gravities of the evolutionary phases.

(iii) *The transformations to observables*: spectra, or colours and bolometric corrections as functions of gravity and temperature, to convert the bolometric luminosity into an SED.

The key feature of the code is to have the three ingredients being allocated in three *independent* sets of matrices. This is very convenient as the code can be used to understand the impact of the various input *selectively* on the final result. We will use this structure to understand the discrepancies between EPS models that are based on different stellar evolutionary tracks. The adopted ingredients are described in the next subsections.

3.1 Energetics

The first matrix contains the energetics, i.e. the luminosities of MS stars and the fuel consumptions of PMS phases. In general, both are taken from stellar evolutionary models, except for those stellar phases that are poorly understood (Section 3.4), for which the energetics are estimated semi-empirically, by means of observations and with the aid of the fuel consumption theorem.

3.1.1 Stellar models

The bulk of input stellar models (tracks and isochrones) is from Cassisi, Castellani & Castellani (1997a), Cassisi, Degl'Innocenti & Salaris (1997b) and Cassisi et al. 2000 (see also Bono et al. 1997). Their main features are summarized in the following. These are *canonical* stellar evolutionary tracks, i.e. the efficiency of the overshooting parameter is assumed to be zero. The actual size of the overshooting has been a matter of debate for several years, and work is in progress to calibrate the overshooting parameter with observational data (Bertelli et al. 2003; Woo et al. 2003). These articles favour moderate amounts of overshooting, but the results on different stellar evolutionary tracks are discrepant. The Cassisi

tracks are used to compute what we will refer to as *standard* SSP models. The choice of these tracks as basis is due to the following reasons: (i) extensive calibrations with galactic GCs have been performed (Cassisi & Salaris 1997; Cassisi et al. 1997b; De Santi & Cassisi 1999); (ii) tracks (isochrones) are provided with very fine time (mass) spacing (e.g. a typical RGB track contains $\sim$5000 models), which is essential to perform good numerical integrations; (iii) these tracks are the closest to the ones (from Castellani, Chieffi & Straniero 1992) that were adopted for the solar metallicity models presented in M98. For the sake of homogeneity, the M98 models have been recomputed with the solar metallicity tracks of the Cassisi's data base. Minimal differences have been found, which are due to the temperature/colour transformations rather than to the stellar tracks. The metallicity of the Cassisi tracks range from $Z_\odot/200$, typical of the Milky Way halo to $2 Z_\odot$, the helium enrichment law being $\Delta Y/\Delta Z \sim 2.5$. In order to extend the metallicity range, we implement a set of tracks with 3.5 solar metallicity, and the same $\Delta Y/\Delta Z$, from the Padova data base (see below). The exact values of helium and metals for the SSP grid are tabulated in the section presenting the results.

Most SSP models in the literature are based on the tracks by the Padova group (Fagotto et al. 1994; Girardi et al. 2000; Salasnich et al. 2000). Therefore, it is interesting to explore the effects of other stellar evolutionary tracks, on the ages and metallicities inferred for real stellar populations. To this aim, several SSPs have been computed by means of the Padova stellar models. The various comparisons will be shown in Section 5. The issue is a very important one as at metallicities above solar, i.e. in the range more relevant to massive galaxies, the calibration of the tracks is hampered by the lack of GCs with ages and chemical compositions known independently.

Finally, the isochrones/tracks of the Geneva data base (Schaller et al. 1992; Meynet et al. 1994) are adopted in order to compute very young SSPs ($10^{-3} \leqslant t < 30$ Gyr).

3.1.2 Main sequence: mass–luminosity relations

Isochrones are adopted up to the turnoff, and the MS luminosity contributions are evaluated by means of equation (2). Therefore, the results depend on the mass–luminosity relations of the isochrones. Fig. 1 compares the mass–luminosity relations of the isochrones from Cassisi and Padova (solid and dotted lines, respectively) for various ages and metallicities. In general, a fairly good agreement is found for masses $\gtrsim 0.5 \, \mathrm{M}_\odot$, independent of the metallicity, while the low MS of the Padova tracks with high metallicity (solar and above) is brighter than that of the Cassisi tracks, by nearly a factor of 2. However, this effect is not important, because the contribution of the low MS to the total light is very small, unless the stellar population has a very steep IMF (e.g. $s \gtrsim 3.5$ in the notation in
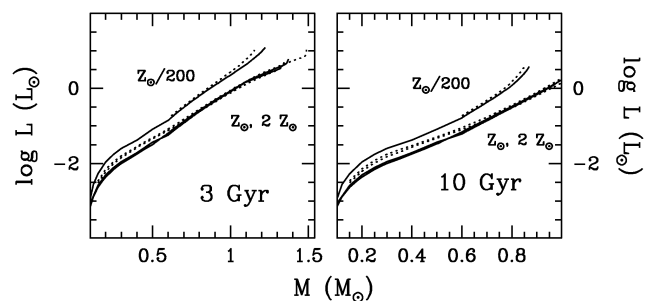

Figure 1. The relation between luminosity and mass for the isochrones of Cassisi (solid lines) and Padova (dotted lines). The metallicities are labelled. Note that the relations for solar and twice solar metallicities nearly overlap.
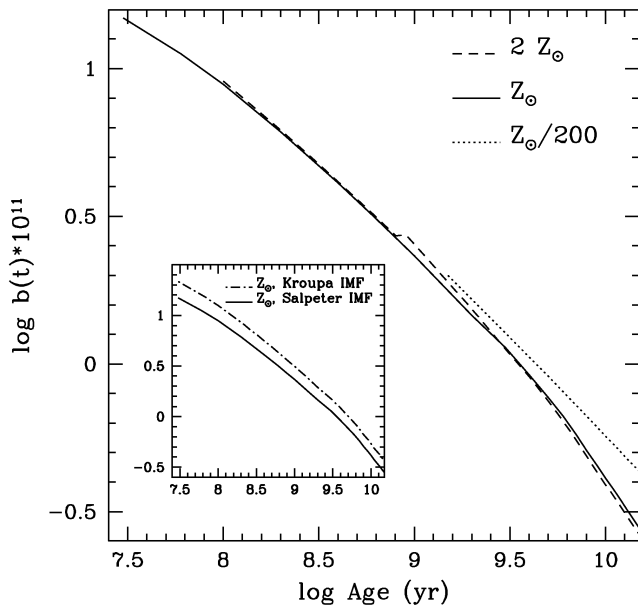
Figure 2. The evolutionary flux $b(t)$ (equation 4) that measures the rate of evolution off the MS, for various metallicities. The $b(t)$ are normalized by means of the IMF scalefactor A in such a way as to be referred to 1 M$_\odot$. The IMF dependence is highlighted in the small internal box, where the $b(t)$ for solar metallicity is shown for the Kroupa and the Salpeter IMF. The Kroupa SSP has a $\sim$30 per cent higher evolutionary rate with respect to the Salpeter SSP.

Figure 3. The stellar evolutionary phases indicated on the observed colour magnitude diagram of the metal-poor Milky Way globular clusters NGC 1851 (data from Piotto et al. 2002). BS stays for 'blue stragglers', a class of stars not included in the evolutionary synthesis. No separation is made between the early and the TP-AGB.

which the Salpeter exponent is 2.35; M98), so that its light is dwarf-dominated. Instead, what is noticeable is the effect of overshooting, because of which the Padova MS has a turnoff mass at given age that is *larger* than that of canonical tracks (e.g. at 3 Gyr and solar metallicity the turnoff masses are 1.45 M$_\odot$ and 1.37 M$_\odot$, respectively). Stellar models with overshooting have more massive convective cores, therefore they run to higher luminosities and live longer than classical models. This effect stems from the higher fuel for a given mass when overshooting is considered, which prolongs the MS lifetime. The effect lasts until the mass has a convective core on the MS, i.e. it disappears for $M \lesssim 1$ M$_\odot$.

As to metallicity effects, at a given mass a higher metal content makes the star fainter, because of the combined effects of the smaller amount of hydrogen and the higher opacity. For example, a 0.8-M$_\odot$ star with 2-Z$_\odot$ metallicity is fainter by a factor of 3 on the MS than one with the same mass but metallicity Z$_\odot$/200. Instead, there is no difference between the solar and twice-solar metallicity MS relations. This comes from the fact that helium increases along with metallicity in both tracks, according to the helium enrichment law $\Delta Y / \Delta Z \sim 2.5$. The higher helium at larger metallicity counterbalances the metallicity effects and keeps the star at roughly the same brightness.

In order to link the PMS evolution of the turnoff mass to its MS, one needs to know the rate of evolution of turnoff-like stars off the MS through the later evolutionary stages, as a function of the SSP parameters (age, metallicity, IMF). According to RB86, this quantity is expressed analytically by the evolutionary flux $b(t)$ (equation 4), which is proportional to the time derivative of the relation turnoff mass/age and the adopted IMF. The dependence of the function $b(t)$ on the SSP parameters is shown in Fig. 2. The main panel focuses on age and chemical composition effects, the small one on the IMF. Obviously, $b(t)$ depends mainly on the age of the
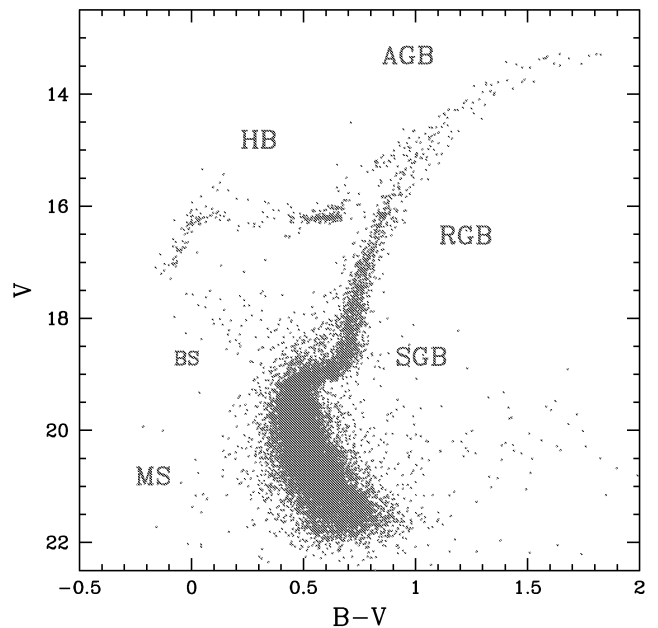
SSP, as the derivative of the turnoff mass does, while metallicity effects have a much milder influence. The effect of the IMF on $b(t)$ was discussed in M98. In brief, the flatter the IMF, the slower $\Psi(M)$ increases with time, so that the rapid decrease in $\dot{M}_{\rm TO}$ dominates for flat IMFs. This results in a steeper SSP luminosity evolution for flatter IMFs. In the small box in Fig. 2 we show $b(t)$ for a Kroupa (2001) IMF, which will be used as alternative choice to the Salpeter one to compute SSP models. The Kroupa (2001) IMF is described as a multiple-part power law, with exponents: 1.3 for $0.1 \lesssim M/M_\odot \lesssim 0.5$ M$_\odot$ and 2.3 for larger masses (in the notation in which the Salpeter exponent is 2.35). The Kroupa IMF has a relatively higher fraction of massive stars, which explains why the correspondent $b(t)$ is steeper than that referred to the Salpeter IMF [note that the $b(t)$ values are normalized to 1 M$_\odot$ of the total mass of the parent SSP and it is the normalization factor that produces the difference].

3.1.3 Post-main-sequence: fuel consumptions

The luminosity contributions of the PMS phases are computed by means of the fuel consumption theorem, according to equation (3). The nomenclature of the main PMS evolutionary phases, in order after the MS, are: subgiant branch (SGB); RGB; helium-burning branch or HB; E-AGB and TP-AGB. The stellar evolutionary phases are highlighted on the observed colour–magnitude diagram of NGC 1851, a metal-poor GC of the Milky Way (Fig. 3: data from Piotto et al. 2002).

In order to compute the fuels, evolutionary tracks are adopted up to the completion of the E-AGB. Complete tracks for the TP-AGB phase are not available. In fact, it is difficult to follow the physics of the stellar interiors during the thermal pulses, and stellar tracks are actually restricted to envelope models (e.g. Renzini & Voli 1981; Iben & Renzini 1983; Lattanzio 1986; Boothroyd & Sackmann 1988; Bloecker & Schoenberner 1991; Marigo, Bressan & Chiosi 1996; Wagenhuber & Groenewegen 1998; Marigo 2001;
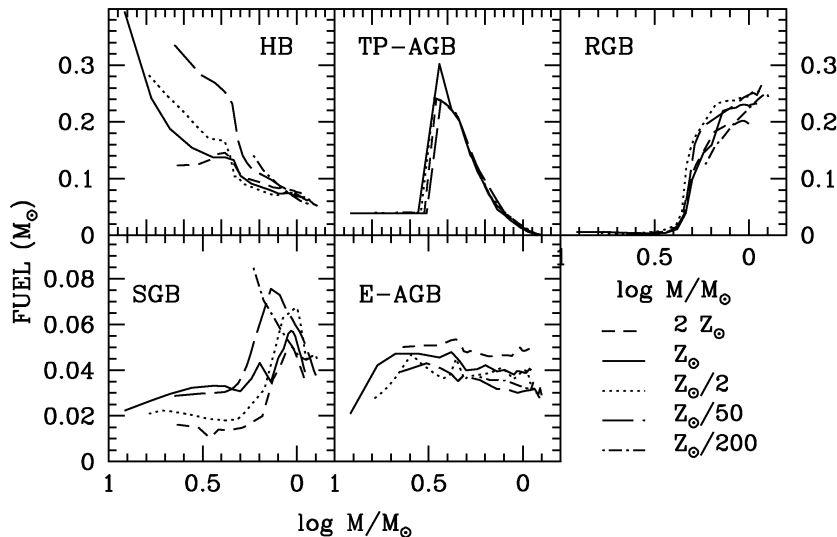
Figure 4. The fuel consumption (in $M_\odot$) in the various PMS phases, as functions of the turnoff mass, for various metallicities.

Mouhcine & Lançon 2002), and even the latter are uncertain due to the occurrence of strong mass-loss that aborts the phase (the *superwind* phase; Iben & Renzini 1983). In the present models the energetics of the TP-AGB comes from the semi-empirical calibration of M98 (see Section 3.4.3).

The fuel for the evolutionary phase *j* (until the E-AGB) is computed by integrating the product of the evolutionary time and the emergent luminosity along the track appropriate to that phase. The tracks for the given turnoff masses are obtained from interpolation in log mass. The evolutionary mass for the helium-burning phase M_{HB} is obtained from M_{TO} after evaluation of the mass-loss during the RGB. This allows playing with various HB morphologies (see Section 3.4). Finally, the separation between HB and E-AGB is set when the mass of the CO core along the track is different from zero. Note that each phase is divided suitably into a certain number of subphases in order to map appropriately the spectral type changes (M98). The criterion for the subdivision into subphases depends on the temperature, therefore, is described in Section 3.2.

Fig. 4 shows the fuel consumption (in $M_\odot$) for the PMS evolutionary phases, as a function of the turnoff mass, for various metallicities. As already pointed out by RB86, the most relevant PMS phase changes with the evolutionary mass, i.e. with the age of the stellar population, and we find here that the trend does not depend on the chemical composition.

In massive stars ($M \gtrsim 3\,M_\odot$), i.e. those dominating *young* – $t \lesssim 0.2$ Gyr – stellar populations, the dominant PMS phase is the HB, its fuel decreases with the decreasing stellar mass. In low-mass stars ($M \lesssim 2\,M_\odot$), i.e. those dominating old – $t \gtrsim 2$ Gyr – stellar populations, the RGB phase is the most important PMS phase, when a He-degenerate core is developed (RB86; Sweigart, Greggio & Renzini 1989). Stars with masses in the narrow mass range between 3 and 2 $M_\odot$, i.e. those dominating $0.2 \lesssim t \lesssim 2$-Gyr old stellar populations, spend a conspicuous amount of fuel on the TP-AGB phase. The onset of the development of the TP-AGB and RGB phases has been called by RB86 'phase transitions'.

The HB fuel (left-hand upper panel) of massive stars is affected by metallicity in the sense of a higher fuel at a lower metal content, owing to the higher relative abundance of hydrogen, an effect similar to that pointed out for the MS luminosity (Section 3.1.2). For example, at masses $\gtrsim 4\,M_\odot$, the $Z_\odot/20$ metallicity has

nearly a factor of 2 more fuel than the solar one. In the small-mass regime ($M \lesssim 1.5\,M_\odot$, $t_{SSP} \gtrsim 3$ Gyr) metallicity effects are negligible.

The RGB phase (right-hand upper panel) starts to develop at masses around 2 $M_\odot$, almost independently of metallicity in these classical (no overshooting) tracks, in excellent agreement with the early findings by Sweigart, Greggio & Renzini (1990). The RGB fuel is rather insensitive to metallicity until $Z_\odot$. For reference, a 10-Gyr $Z_\odot/200$ stellar population has 0.24 $M_\odot$ of RGB fuel and a coeval one with solar metallicity 0.23 $M_\odot$. However, at higher metallicities the RGB fuel starts decreasing with increasing metal content, and, for example, a stellar population with 3.5 $Z_\odot$ (see Fig. 5) has 0.15 $M_\odot$ of RGB fuel, nearly 35 per cent less than the solar chemical composition. This is the effect of the very high helium abundance associated to the high metal content because of the helium enrichment law $\Delta Y/\Delta Z \sim 2.5$, which reduces the amount of hydrogen, i.e. the RGB source of fuel, drastically. A discussion on the effect of helium abundance on the fuel of PMS phases is found in Greggio & Renzini (1990).

The TP-AGB fuel consumption (middle upper panel) is one of the most conspicuous, together with that in HB and RGB, and is a strong function of the stellar mass, therefore of the age of the stellar population. It reaches a maximum for masses between 3 and 2 $M_\odot$ and is negligible for masses outside this narrow intermediate mass range. Furthermore, the TP-AGB fuel consumption does not depend appreciably on metallicity (see Section 3.4.3).

Finally, the SGB and E-AGB (lower panels) are the least important phases, providing at most $\sim$20 per cent and $\sim$10 per cent, respectively, of the total PMS luminosity (see also Section 4.1).

Fig. 5 shows the total fuel consumption in the whole PMS, as a function of age, for the various metallicities. In interpreting this figure in a stellar population perspective, it is useful to remind oneself that the fuel scales directly with the PMS luminosity of a stellar population.

The effect of the chemical composition that we discussed previously is evident on the total fuel of stellar populations with ages smaller than $\sim$1 Gyr, which is larger the lower the metal content. A young metal-poor stellar population with $Z = Z_\odot/20$ has $\sim$20 per cent more fuel to be burned, e.g. is 20 per cent brighter than a coeval one in which the metallicity is twice solar. In older stellar
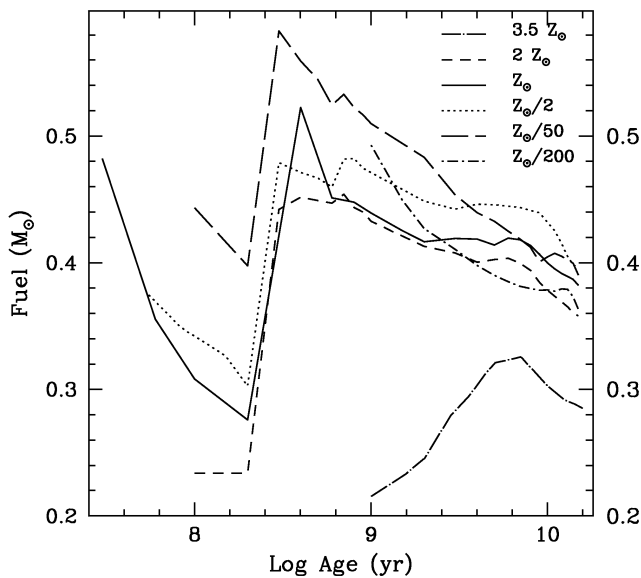
Figure 5. The total fuel consumption (in $M_\odot$) in the whole PMS, as a function of the age of the SSP, for the various metallicities. Note that the fuel scales directly with luminosity. The metal-rich SSP of the Padova data base (long-dashed/dotted line) sticks out for having a very small amount of fuel. The TP-AGB phase is not included in this SSP.
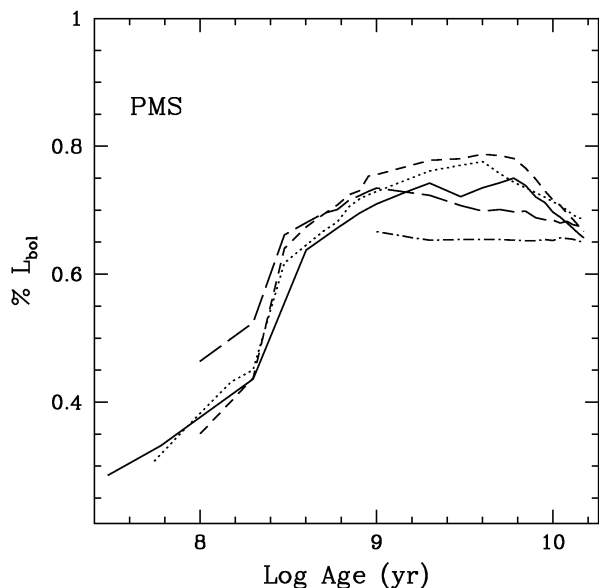

Figure 6. The luminosity contributions of the PMS (evaluated with equation 3) for the various metallicities (line styles as in the previous plots) and Salpeter IMF.

Figure 7. Influence of the stellar tracks. Comparison between the EPS ingredients obtained with classical (solid line, from Cassisi et al.) and overshooting tracks (dotted line, from Girardi et al. 2000; Salasnich et al. 2000). From top left to bottom right the various panels show: the total fuel consumption (in $M_\odot$) for the various PMS phases, as a function of the age of the SSP; the evolutionary flux; the bolometric luminosity of MS and post-MS. For both tracks the metallicity is half-solar ($Z = 0.008$), and only ages larger than 0.3 Gyr are plotted. The TP-AGB fuel is not considered for this comparison since it does not depend on the adopted tracks, as explained in the text.

populations metallicity effects become less important, as a consequence of the small metallicity dependence of the RGB fuel, that is, the largest source of energy at high ages. However, an exception is the metal-rich stellar population ($Z = 3.5\,Z_\odot$, dash-dotted line), which at old ages has $\sim$25 per cent less fuel than all other chemical compositions, for which the fuel scatter around a value $\sim$0.4 $M_\odot$. This is due to the very high abundance of helium in these tracks, caused by the assumed helium enrichment law ($\Delta Y / \Delta Z \sim$ 2.5), which implies the abundance of hydrogen to be only 0.45. This explains the sharp decrease in fuel consumption since hydrogen is its most important source.
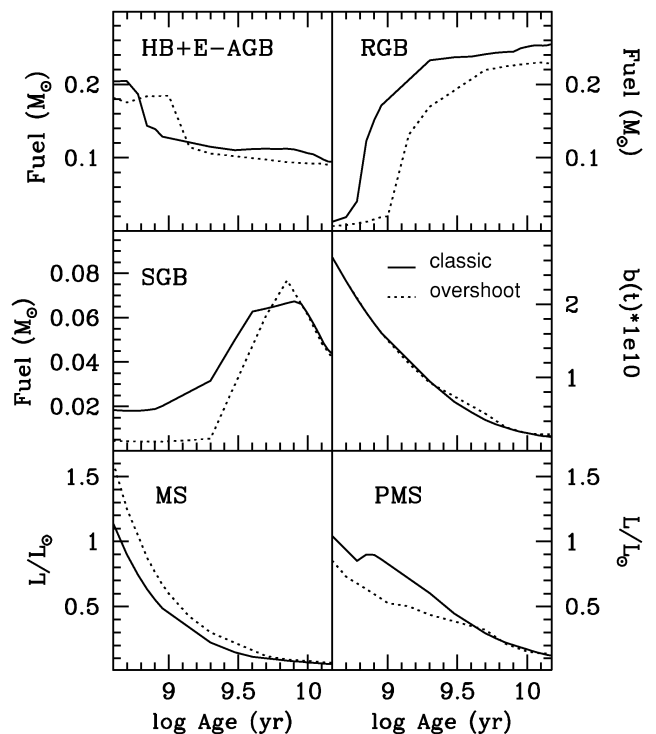
The sizable increase of PMS fuel consumption at ages around 0.3 Gyr ($\log t \sim 8.47$) marks the onset of the AGB phase transition that is dominated by the TP-AGB (M98, Fig. 4). At greater ages the RGB phase transition occurs, which is barely visible in Fig. 5 as a small bump around 1 Gyr due to the simultaneous decrease of TP-AGB fuel. Finally, the bumps in the fuels at late ages ($t \gtrsim 6\,\mathrm{Gyr}$) reflect the trend of the SGB fuel (Fig. 4). After the development of the TP-AGB, $\sim$70 per cent of the total energy of a stellar population comes from PMS stars (Fig. 6).

The dependence of MS and PMS energetics on stellar evolutionary tracks is illustrated in Fig. 7. The transition from a non-degenerate to a degenerate helium core that marks a well-developed RGB phase and a drop in the HB fuel occurs at later epochs if overshooting is taken into account in the stellar models. This is shown in the top panels of Fig. 7, where the fuels obtained with classical (solid) and overshooting (dotted) tracks as functions of the age of the stellar populations are compared. The RGB phase transition occurs at 0.7 Gyr in classical models and at 1 Gyr in models with overshooting.

The age marking the onset of the RGB phase transition was early recommended by Barbaro & Pigatto (1984) as a suitable observational check of the overshooting hypothesis. This test has been recently performed by Ferraro et al. (2004), where deep, VLT-based, *JHK* CMDs of LMC GCs allow the quantification of the population ratios between RGB and the He-clump, as functions of the GC

age. The comparison with the theoretical predictions of classical and overshooted tracks (the same tracks shown in Fig. 7) clearly exclude the latter, in that they predict a substantially later development of the RGB (see figs 8 and 9 in Ferraro et al. 2004). This result supports our use of classical evolutionary tracks for our standard SSP models. Fig. 7 (bottom left-hand panel) also shows that the MS luminosity of the tracks with overshooting is larger than that of the classical one, while the trend is reversed for the PMS (bottom right-hand panel), for the reasons already explained. Note that the evolutionary fluxes are very similar (central right-hand panel), which is mostly due to the similarity of the time derivative of the turnoff masses. Finally, the SGB phase appears also to be a little delayed (central left-hand panel), but its impact on the results is very small.

Because of the earlier RGB phase transition, at $t \sim 1$ Gyr the SSPs based on the Cassisi tracks are nearly 40 per cent more luminous than those based on the Padova tracks. An output that is affected by these variations is obviously the M/L ratio, a key quantity used to determine the stellar mass of galaxies (see Section 4.4).

3.2 Temperatures

The second matrix contains the distribution of effective temperatures and surface gravities of the evolutionary phases j for the various ages and metallicities. As already mentioned, every evolutionary phase is split into a certain number of so-called *photometric subphases*, inside which the spread in effective temperatures $T_{\rm eff}$ is $\lesssim 100$ K. This was found to be appropriate for a good tracing of the varying spectral type along a phase.[1] What is relevant to evolutionary synthesis models is that the fuel consumption is evaluated specifically in each subphase. In general, the consumption of energy is not homogeneous with temperature. This is visualized in Fig. 8, where the temperature/gravity subphases for old (12 Gyr) RGBs and HBs are displayed for two metallicities (circles for solar; triangles for [Z/H] = −2.25), with the symbol size being proportional to the fuel. The fuel consumption along the RGB of a metal-rich stellar population is enhanced at the so-called RGB *bump* (big circles in the left-hand panel of Fig. 8), when the H-burning shell reaches the internal layer that was previously mixed through the first convective dredge-up, gets fresh fuel and therefore spends a longer time in this location (Sweigart et al. 1989). The RGB bump is rather close to the He clump. If the total RGB fuel was assigned homogeneously along the RGB track, the weight of the bump would be unappropriately distributed along the whole track, particularly at the tip, with the effect of overestimating the near-IR flux of the SSP. The fuel consumption approach implemented here, where the evolutionary time-scale is considered, is an efficient way of taking the bump into account. The bump is predicted to almost disappear at decreasing metallicity (Sweigart et al. 1989), and indeed the RGB fuel in the metal-poor stellar population results to be rather homogeneously distributed (triangles in Fig. 8). Note that the significant contribution of the RGB tip to the fuel comes from the high luminosity of that subphase.

The right-hand panel of Fig. 8 illustrates the effect of the HB morphology on the temperature of the subphases. For the same ages and metallicities, two options for the HB morphology are shown, red (open symbols) and blue (filled symbols). We remind that blue/red HBs mean that the whole HB lifetime is spent on the blue/red side of the RR Lyrae strip, while intermediate HB is used to refer to
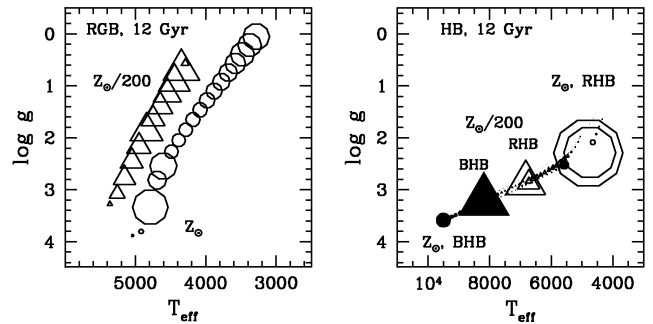

Figure 8. Relation between fuel consumption and temperature subphases. The left-hand panel shows the subphases along the RGB of 12 Gyr SSPs with solar and $Z_\odot/200$ metallicities (circles and triangles, respectively). The right-hand panel shows the subphases along the HB for the same metallicities, filled and open symbols refer to blue and red horizontal branch (RHB) morphologies, respectively. In both panels the symbol sizes scale with the fuel consumptions. The big circles in the left-hand panel correspond to the position of the so-called RGB bump.

the mixed cases.[2] In order to trace the HB evolution properly, we use the evolutionary track for the helium-burning phase of the mass that is obtained after mass loss is applied to the RGB track (see Section 3.4.2). In the HB phase, most fuel consumption occurs on the so-called zero-age helium burning (ZAHB) that usually corresponds to a very narrow temperature range, the evolution from the tip-RGB to the ZAHB and from the ZAHB to the E-AGB happening on very short time-scales ($\sim$1 Myr). However, in presence of a strong mass-loss like in the case of a BHB at high Z (filled circles) the evolutionary time-scale can be significant at various temperature locations.

Stellar effective temperatures depend crucially on the efficiency of convective energy transfer, parametrized by the mixing length parameter α. The latter cannot be derived from first principles, and as far as we know it could be connected to several stellar parameters, such as the stellar mass, the evolutionary status or the metallicity, and its calibration with observational data is certainly required. The use of uncalibrated theoretical effective temperatures in EPS computations is extremely dangerous, as α is the synchronization of the EPS clock (RB86).

The calibration of the mixing length for the Cassisi tracks is described in Salaris & Cassisi (1996). The tracks with solar metallicity are computed for $\alpha = 2.25$, a value that matches the Sun. This same value is kept in the tracks with supersolar metallicities (Bono et al. 1997). At subsolar metallicities, however, the mixing-length parameter is not assumed to be the same, but to vary with Z, such that the temperatures of the RGB tips of Milky Way GCs are reproduced. The values range from 2 to 1.75, with a trend of decreasing mixing length with metallicity (see table 2 in Salaris & Cassisi 1996). In the Girardi et al. (2000) tracks from the Padova data base, however, the same value of the mixing-length parameter that is calibrated with the Sun is assumed at all metallicities.

The resulting differences in the RGB temperatures are shown in Fig. 9, where the RGBs of old (10 Gyr) isochrones from

---

[1] It should also be noted that model atmospheres are provided with $\Delta T_{\rm eff} \sim 200$ K.

[2] Traditionally, the separation between red and blue HBs was assigned on the basis of the location of the RR Lyrae stars in metal-poor Milky Way GCs (Dickens 1972), whose typical temperature is $T_{\rm eff} \sim 7000$ K. BHBs are those in which most of the stars are found at temperatures hotter than $T_{\rm eff\,RRLyrae}$, red horizontal branches (RHBs) when most of the stars lie at cooler temperatures, intermediate horizontal branches (IHBs) for the mixed cases.
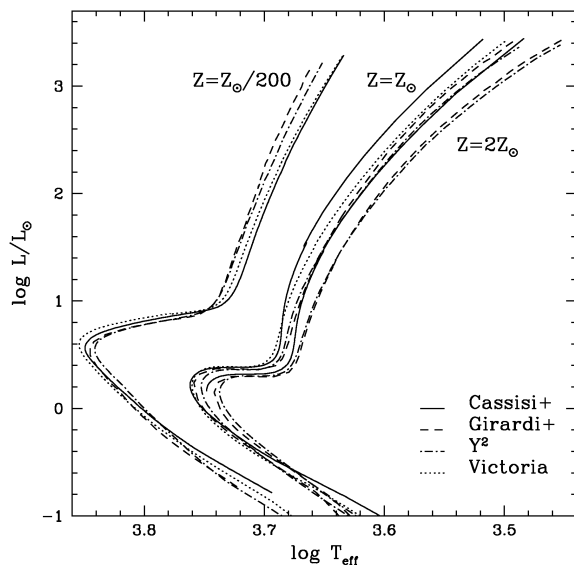
Figure 9. Influence of the stellar models on RGB temperatures. For metallicities $Z_\odot/200$, $Z_\odot$, $2Z_\odot$, classical (solid line, from Cassisi et al.) and overshooting tracks (dotted line, from Girardi et al. 2000) are shown up to the RGB tip. The Padova tracks of Girardi et al. (2000) have cooler RGBs at high metallicity (solar and above) and warmer ones at low metallicities. At least part of this effect should arise from the adopted mixing-length parameter. Also plotted are the isochrones from the Victoria group (dotted line, VandenBerg et al. in preparation, for solar metallicity; Bergbusch & VandenBerg (2001) for subsolar metallicities) and from Yale (Y^2, dashed line, Yi et al. 2003). All models have the age of 10 Gyr.

Cassisi et al. (solid lines) and from Padova (Girardi et al. 2000, dotted lines) are shown for three metallicties ($Z_\odot/200$, $Z_\odot$, $2Z_\odot$, from left to right). At high metallicities, the Padova RGBs are cooler than those of the Cassisi's tracks, in such a way that the 2-$Z_\odot$ RGB of Cassisi coincides with the solar one by Girardi et al. Since the cooler temperatures are proper to the whole RGB, and not only to the tip, from what was said before (see also Fig. 8) it has to be expected that the optical/IR flux ratio of metal-rich SSP models will depend on the choice of the tracks. This effect will be quantified in Section 5. Unfortunately, as already mentioned, at these high metallicities, which are the most relevant to massive galaxies, the calibration of the models is hampered by the lack of metal-rich GCs with independently known ages and metallicities. The only two objects useful to this purpose are the two metal-rich GCs of the Baade window (NGC 6553 and 6528, Ortolani et al. 1995), whose total metallicity is around solar (Thomas et al. 2003a). The complication here is that these two objects have enhanced [α/Fe] ratios (Barbuy et al. 1999; Cohen et al. 1999), therefore the proper calibration requires the use of stellar tracks accounting for this effect. Element ratio effects are being incorporated in stellar models (e.g. Bergbusch & VandenBerg 1992, 2001; Salasnich et al. 2000; Kim et al. 2002), but for the stellar tracks considered here, their [α/Fe]-enhanced version was either not yet available at the time these models were computed (Cassisi's tracks) or does not appear to be convincing (see Thomas & Maraston 2003 for the Salasnich et al. 2000 tracks).

At lower metallicities the opposite effect is found, i.e. the Cassisi tracks appear to have cooler RGBs than the Padova ones. At least part of the effect must originate from the treatment of the mixing length. However, the methodology by Salaris & Cassisi (1996) depends necessarily on temperature/colour transformations, as the RGB theoretical temperature luminosity relation must be converted

into the observed colour–magnitude diagram. Therefore, it is hard to push any strong conclusion on which parametrization of the mixing length is better. Generally, any calibration of stellar tracks depends upon the adopted temperature/colour transformations, and in particular for the coolest part of the RGB these are notoriously uncertain.

The comparison with the Padova tracks is the most relevant to EPS issues, since these tracks are adopted by all existing EPS codes except the one presented here. However, several other isochrones exist in the literature. In Fig. 9 the latest Yale models (Y^2; Yi, Kim & Demarque 2003) and the models of Victoria (VandenBerg, private communication, for solar metallicity; Bergbusch & VandenBerg 2001 for the subsolar metallicity) are shown. Both sets of tracks include overshooting. The Y^2 isochrones (dot-dashed) behave very similarly to the Padova ones at all metallicities. At solar metallicity the Victoria models (dotted line) agree quite well with the Cassisi's one till the early portion of the RGB, after which the track departs towards cooler temperatures reaching values around the tip that are more similar to those of the Padova or Yale isochrones. Interestingly the metal-poor isochrone of Victoria has a RGB rather similar to that of Cassisi, which suggests that the calibration of the mixing length is not the whole story. At supersolar metallicities the Victoria isochrones are not available. In Section 5 we will show the impact of the various RGBs on the integrated colours of SSPs.

3.3 Transformations to observables

The third matrix contains the transformations to the observables, used to convert effective temperatures and surface gravities into a SED. The transformations can be either theoretical or empirical. The models of M98 used a mix bag of ingredients. They rely on the classical Kurucz (1979 and revisions) model atmospheres for $3500 \lesssim T_{\rm eff}\,({\rm K}) \lesssim 35\,000$, complemented with models for M giants by Bessel et al. (1989) for cooler temperatures, and with empirical colours for TP-AGB stars (see M98 for references). The models presented here are partially revised in this respect because the ingredients of the mixed matrix constructed by M98 have been in the meantime compiled into one library (see Section 3.3.1), in which border effects between the merged libraries are considered in far more detail than it was done in M98. Also the empirical ingredients for TP-AGB stars have been revised, because of the availability of complete SEDs (Section 3.3.2).

3.3.1 Model atmospheres

The synthetic stellar spectra are taken from the spectral library compiled by Lejeune, Cuisinier and Buser (1998, in its latest version as available on the web, hereafter the BaSel library). This library has become widely used in population synthesis studies and was obtained by merging the Kurucz library of model atmospheres ($T_{\rm eff} \gtrsim 3500° $ K) with model atmospheres for cooler stars (for references and full details see Lejeune et al. 1998). As in M98, a quadratic interpolation in ($T_{\rm eff}$, $\log g$) is performed on this library to compute the stellar spectra appropriate to each subphase. The BaSeL library is provided for various iron abundances. We obtain the appropriate one to each set of tracks by interpolating linearly in [Fe/H]. Finally, a blackbody spectrum is assigned to $T_{\rm eff} \gtrsim 50\,000$ K. The use of the BaSel library allows the computation of model SEDs with low spectral resolution, i.e. 5–10 Å up to the visual region, 20–100 Å in the near-IR. Bruzual & Charlot (2003) adopt STELIB (Le Borgne et al. 2003, see also Le Borgne et al. 2004), an empirical spectral library of stars with metallicity around solar and a much higher spectral resolution (3 Å), to compute a set of SSPs with solar metallicity. They compare the integrated colours $B - V$ and $V - K$ obtained

with both BaSel and STELIB. The colour differences as induced by the spectral transformations result to be at most a few hundredths of magnitude in a wide range of ages.

3.3.2 Empirical spectra for TP-AGB stars

As is well known, current synthetic spectral libraries do not include spectra for carbon-rich and oxygen-rich stars populating the TP-AGB phase, although some theoretical computations begin to be available (Lloidl, Lançon & Jorgensen 2001). For the spectra of this type of stars we use the empirical library by Lançon & Mouhcine (2002). The latter is based on the library of individual stellar spectra by Lançon & Wood (2000), that collects observations of C- and O-type stars in the Milky Way and Magellanic clouds. Since individual stellar spectra of such cool, variable stars are subjected to strong star-to-star or observation-to-observation variations, Lançon & Mouhcine (2000) have constructed mean templates of the Lançon & Wood (2000) library, obtained by averaging observations of individual stars. In this work we will use the average templates.

3.4 Recipes for critical stellar phases: TP-AGB and HB

3.4.1 Mass loss in red giants

The stellar temperatures and luminosities during those evolutionary phases that follow episodes of, or suffer themselves from, stellar mass loss, cannot be predicted by stellar tracks. This comes from the fact that a theory relating mass-loss rates to the basic stellar parameters does not exist. Therefore, mass loss has to be parametrized and its efficiency calibrated with data. Due to such a complication we call these stellar phases 'critical'. The amount of mass loss is usually parametrized by means of the Reimers (1977) empirical formula $dM = -\eta[L/(R \log g)] \, dt$, where M, L, $\log g$, R stand for mass, emergent luminosity, surface gravity and radius, respectively, of the stellar configuration in its lifetime dt. The parameter η introduced by Fusi Pecci & Renzini (1976) takes into account the efficiency of mass loss. In stars of intermediate mass ($2 \lesssim M/M_\odot \lesssim 8$), mass loss significantly influences their PMS evolution, i.e. the energetics and the temperature, along the TP-AGB (Section 3.4.3). In low-mass stars ($M \lesssim 2 \, M_\odot$) mass loss occurs also during the RGB, particularly towards the tip, affecting the subsequent HB evolution and hence the HB morphology (Section 3.4.2).

It is important to note that the efficiency η cannot depend too much on metallicity (Renzini 1981), because the observed HB morphology of GCs is almost always red at high-metallicity, implying that mass loss does not increase significantly with the metal abundance. Renzini (1981) evaluates $\eta \propto Z^x$, $x \lesssim 0.2$.

In the following sections we describe the modelling of HB and TP-AGB.

3.4.2 The horizontal branch morphology

The amount of mass loss during the RGB phase is computed by integrating the Reimers formula along the RGB track. The efficiency η was calibrated by Fusi Pecci & Renzini (1976) by comparing the mass of RR Lyrae in the instability strip of the metal-poor MW GC M13 ([Z/H] ~ -1.5), with its turnoff mass, and found to be ~ 0.33. This value of η is by definition appropriate only at this metallicity and for the RGB tracks used by Fusi Pecci & Renzini (1976), and it has to be re-obtained for other chemical compositions and when other stellar models are used.

The approach followed by Maraston & Thomas (2000) was to compute the integrated Hβ line that is very sensitive to the

HB morphology (see also de Freitas Pacheco & Barbuy 1995; Barbaro & Poggianti 1997; Lee, Yoon & Lee 2000) and to compare it with galactic GCs of known ages, metallicities and HB morphologies. The value of η appropriate to [Z/H] ~ -2.25 was found to be 0.2.

The procedure of using one value of η per metallicity (and age) aims at recovering the average trend of a bluer HB morphology with decreasing metallicity, the latter being the first parameter ruling the HB morphology. The trend is easy to understand in terms of stellar evolution. At low metallicity the evolutionary mass is smaller at a given MS lifetime (because the stars are more compact and hotter and the nuclear burning is more efficient), therefore the production of hotter effective temperatures by envelope removal is easier (helped also by the lower metal content). However, as is well known, a large scatter is found in the HB morphology of GCs with the same nominal metallicity, a yet unexplained fact that is recalled as the second parameter effect. The account of all possible HB morphologies in a SSP model is not useful, but it is sensible to provide models with a few choices for the HB morphology that are able to encompass the observed average trend and scatter.

The adopted values of η are $\eta = (0.2; 0.33)$ at [Z/H] $= (-2.25; -1.35)$. The correspondent amount of mass loss along the RGB is shown in Fig. 10, where the mass difference (in $M_\odot$) between the turnoff mass and the mass in the HB phase is shown as function of age for the two adopted η values. These values are in remarkable agreement with those computed by Greggio & Renzini (1990) using a different set of evolutionary tracks. The resulting HB morphology is shown in Fig. 11 by means of the percentage of fuel burned at $T_{\rm eff} \gtrsim 7000$ K, according to the definition of BHB given in footnote 2, Section 3.2. The HB morphology is almost completely blue (BHB) at [Z/H] $= -2.25$ and $t \gtrsim 10$ Gyr, and at [Z/H] $= -1.35$ and $t \gtrsim 14$ Gyr. The morphology is red (RHB) at ages lower than 6 Gyr for [Z/H] $= -1.35$, intermediate (IHB) otherwise. At [Z/H] $= -2.25$, the HB morphology is never completely red, because the metallicity is so low that the HB track spends a non-negligible amount of fuel bluewards of the RR Lyrae strip even
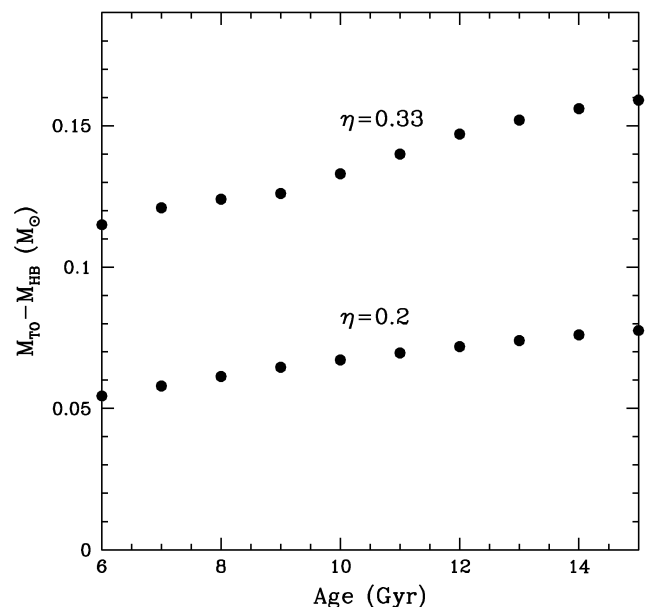

Figure 10. The amount of mass loss along the RGB, expressed as the mass difference between the turnoff mass and the mass at the Helium-burning stage, as function of age for two mass loss efficiency η.
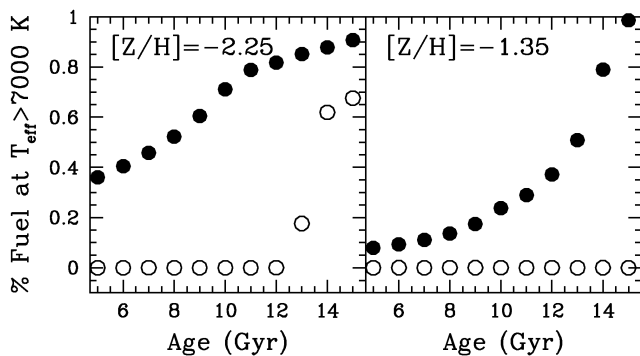
Figure 11. The HB morphology as function of age and metallicity that results from having applied $\eta = 0.2$ and 0.33 at $[Z/H] = -2.25$ and $[Z/H] = -1.35$, respectively (filled symbols). The y-axis gives the percentage of the total HB fuel that is spent at $T_{\rm eff} \gtrsim 7000$ K. The open symbols show the resulting fuel partition when no mass loss is applied during the RGB evolution.

without mass loss (open symbols in Fig. 11). The effect of age is such that the higher the age is, the lower is the stellar mass and the higher is its effective temperature for the same mass loss. Therefore, at a given η the HB morphology gets bluer with increasing age (see also Lee et al. 2000). The SSP models computed with these choices of η have been proven to give a very good match of the Hβ line and the mid-UV spectra (Maraston & Thomas 2000) and of the higher order Balmer lines (Maraston et al. 2003) of Milky Way GCs as function of their total metallicities.

At higher metallicities, the HB of Milky Way GCs is found to be red in almost all cases. However, we know at least two examples of metal-rich GCs that have extended HB morphologies. These are the bulge GCs NGC 6441 and GC 6388 (Rich et al. 1997) with $[Z/H] \sim -0.55$. As shown in Maraston et al. (2003), the models by Maraston & Thomas (2000) were able to reproduce the observed Balmer lines of these two clusters by assuming moderate mass loss along the RGB, implying 10–15 per cent of fuel to be spent blueward the RR Lyrae strip. This fraction is consistent with the observed value.

The finding of Rich et al. (1997) calls for the need of models with BHBs also at high metallicities. For this purpose we seek the η value at which the HB fuel is spent (almost) entirely blueward of the RR Lyrae strip. For the Cassisi tracks we find $\eta = (0.85, 0.45)$; $(1.0, 0.7)$; $(0.94, 0.66)$ for 10 and 15 Gyr and metallicities half-solar, solar and twice solar, respectively. The masses at the HB phase are then ~ 0.5–0.55, whose temperatures reach ~ 9000 K. This amount of mass loss results in the removal of nearly half of the initial stellar mass during the RGB. Note finally that by choosing a larger η, one gets an even bluer HB morphology. The SSPs with high-Z and BHB are computed for the ages of 10 and 15 Gyr.

As a last remark, the variation in the HB fuel between models with and without mass loss is that there is less fuel in the models in which mass loss is applied, which stems from the lower evolutionary mass (see Fig. 4). Such differences amount to roughly 7 per cent at $[Z/H] = -2.25$, to 15 per cent at $[Z/H] = -1.35$, to 27 per cent at half-solar metallicity, to 40 per cent at solar metallicity and to 54 per cent at 2 Z$_\odot$.

3.4.3 The thermally pulsing AGB: inclusion in the integrated spectra

M98 present SSPs in which the TP-AGB phase was included semi-empirically in the models, using a table of theoretical fuel consump-

tions (from Renzini 1992) and calibrating them with measurements of the bolometric contribution of the TP-AGB phase to the total light in intermediate age LMC GCs (from Frogel, Mould & Blanco 1990, see fig. 3 in M98). Basically, the observed contributions fix the left-hand-side member of equation (3) written for j = TP AGB, which allows the evaluation of the fuel, using the evolutionary flux appropriate for the given age. This calibration of the fuel allows one to determine empirically the mass-loss efficiency along the TP-AGB phase, which is found to be $\eta \sim (1/3)$–$(2/3)$.

Maraston et al. (2001a) extend the SSP models to half and twice solar metallicity, introducing an analytical recipe that connects the amount of TP-AGB fuel to the envelope mass at the first thermal pulse (beginning of the TP-AGB phase). Briefly recalling, the fraction of envelope mass that is burned as TP-AGB fuel is determined for the turnoff masses at solar metallicity from the fuel table of M98. As a next step, the relations between envelope and total masses for the turnoff stars with different chemical compositions (taken from the stellar tracks at the termination of the E-AGB) are used to establish which fractions of them goes into TP-AGB fuel as function of metallicity. In this scaling it is assumed that the mass-loss efficiency (which is derived from the Magellanic Cloud GCs) does not depend on metallicity. As a result of this assumption together with the fact that the turnoff mass is rather insensitive to metallicity, the total TP-AGB fuel does not depend too much on the chemical composition (Maraston et al. 2001a, see Fig. 4). This is a robust result for two reasons. (1) Mass loss is not affected significantly by metallicity, as we discussed in the previous section. (2) The TP-AGB fuel decreases very little with increasing mass-loss efficiency. Renzini & Voli (1981) show that by doubling η from 0.33 to 0.66 the fuel of a 2-M$_\odot$ star with solar metallicity decreases by only 20 per cent.

Instead the metallicity influences the partition of the total fuel between C and M stars, according to the rationale of Renzini & Voli (1981, adopted in both M98 and Maraston et al. 2001a). Briefly summarizing, in metal-poor chemical compositions the abundance of oxygen in the envelope is lower and a lower amount of carbon has to be dredged up in order to reach C/O > 1, hence binding all the oxygen into CO molecules (those with the highest binding energy). The residual carbon is then available to produce CH, CN
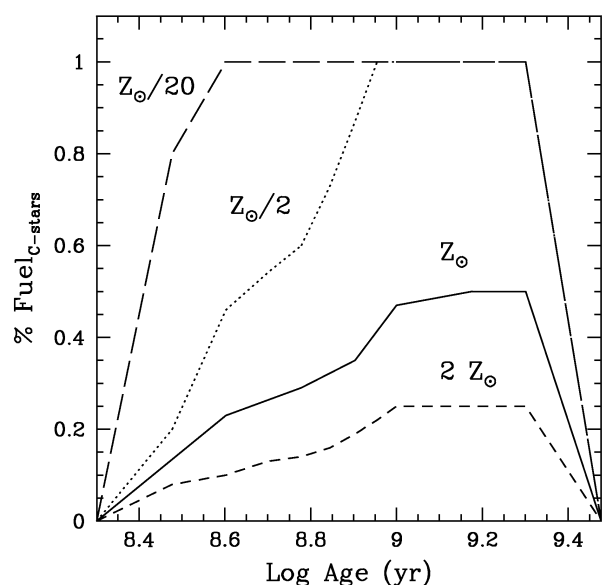

Figure 12. The percentage of the TP-AGB fuel spent in carbon star mode for the various metallicities, as a function of age.

and C_2 molecules, and carbon stars are made. Therefore, a metal-poor stellar population is expected to have more carbon stars than a metal-rich one. Quantitatively, the fuel in C-stars doubles by halving the metallicity. The adopted recipe is given in Fig. 12, where the percentage of the TP-AGB fuel that is spent by carbon-type stars as a function of metallicity is shown. The reference metallicity to which the scaling of Renzini & Voli (1981) is applied, is the 0.5 $Z_\odot$ metallicity (dotted line), because this is the chemical composition of the Magellanic cloud GCs that are used as calibrators.[3] Solar and twice solar metallicities (solid and short-dashed line, respectively) are assigned half and one quarter of the fuel in C-star of the 0.5 $Z_\odot$ metallicity, respectively.[4] At [Z/H] ~ -1.35 (long-dashed line) the fuel in C-star is a factor of 10 larger than at 0.5 $Z_\odot$, therefore the TP-AGB fuel is almost always spent by C stars. Finally, at [Z/H] ~ -2.25 all of the TP-AGB fuel is assigned to C-stars. These numbers can be compared to data of resolved C-stars in galaxies and help to constrain the age distribution of the stellar populations. For example, Davidge (2003) finds that the C-star component is 10 per cent of the whole AGB in the dwarf galaxy NGC 205. According to Fig. 12 this implies that either a burst has occurred less than ~ 200 Myr ago (as favoured by Davidge 2003) or the stellar population is globally old. Also interesting is the finding of a conspicuous population of C stars in the arms of M33 (Block et al. 2004), which could help constraining the star formation history of this galaxy.

Note that the C/M ratio as a function of metallicity by Renzini & Voli (1981) is confirmed by the recent TP-AGB models of Marigo, Bressan & Chiosi (1999), as inferred from their figures since quantities are not tabulated. Our previous models were restricted to broadband colours due to the unavailability at the time of spectra, either theoretical or empirical, appropriate to TP-AGB stars. However, in order to be useful for high-redshift studies, the TP-AGB phase has to be included in the synthetic SED. This improvement of the models is performed here. The fuel is distributed among the empirical spectra of the individual C- and O-type stars by Lançon & Mouhcine (2000). The spectral type that starts the TP-AGB phase is chosen to be close to that of the subphase terminating the E-AGB phase. Spectral types of both O-and C-stars are then included, as described above.

4 RESULTS

The model outputs are the integrated spectrophotometric properties of SSPs, namely, SEDs, broad-band colours (in Johnson–Cousins, Sloan, *Hubble Space Telescope* filter systems), spectral line indices, mass-to-light ratios, bolometric corrections, etc. These are functions of the main parameters of the SSP model: the age t and the chemical composition X, Y, Z (refereed to as [Z/H]).[5] Ages and metallicities of the SSP grid are listed in Table 1. Models are

---

[3] Frogel et al. (1990) measure also the luminosity contributions of C and M-type stars as functions of the GC age.

[4] L. Greggio and M. Mouchine pointed out that the percentage of fuel spent as C and M stars in Table 4 and Fig. 2 of (M98) is reversed. This mistake concerns only the graphics and not the models. In any case the reader is referred to the present Fig. 12 and to the tables provided at the model web page.

[5] The notation [Z/H] is used to indicate total metallicities, i.e. the total abundance of heavy elements with respect to hydrogen normalized to the solar values, i.e. [Z/H] $= \log (Z/Z_\odot) - \log (H/H_\odot)$. By [Fe/H] we mean the abundance of iron with respect to hydrogen normalized to the solar values, i.e. [Fe/H] $= \log(Fe/Fe_\odot) - \log (H/H_\odot)$. If elements have solar proportions then [Fe/H] $=$ [Z/H]. In case of α-element enhancement, the

Table 1. Ages, metallicities and input tracks of the SSP grid.

t (Gyr)	(Y, Z)	[Z/H]	Stellar tracks
1–15	0.230, 10^{-4}	−2.25	Cassisi
3×10^{-6} to 15	0.230, 0.001	−1.35	Cassisi + Geneva
3×10^{-6} to 15	0.255, 0.01	−0.33	Cassisi + Geneva
3×10^{-6} to 15	0.289, 0.02	+0.00	Cassisi + Geneva
3×10^{-6} to 15	0.340, 0.04	+0.35	Cassisi + Geneva
1–15	0.390, 0.07	+0.67	Padova

Table 2. HB morphologies of the SSP grid.

[Z/H]	Age (Gyr)	η_{massloss}	HB morphology	Ref.
−2.25	<=12	0.00	RHB	RI-HB
−2.25	>12	0.00	IHB	RI-HB
−2.25	<10	0.20	IHB	IB-HB
−2.25	>=10	0.20	BHB	IB-HB
−1.35	all	0.00	RHB	RI-HB
−1.35	10–13	0.33	IHB	IB-HB
−1.35	14–15	0.33	BHB	IB-HB
−0.33	all	0.00	RHB	RI-HB or IB-HB
−0.33	10, 15	0.55	BHB	high-Z BHB
0.00	all	0.00	RHB	RI-HB or IB-HB
0.00	10, 15	0.55	BHB	high-Z BHB
0.35	all	0.00	RHB	RI-HB or IB-HB
0.35	10, 15	0.55	BHB	high-Z BHB

generally given in time steps of 1 Gyr, for ages larger than 1 Gyr, and of 0.1 Gyr for smaller ages. The table indicates also the source for the input stellar tracks/isochrones, according to the description and references given in Section 3.1. Model assumptions concern the IMF and the morphology of the HB. The models are computed for two choices of the IMF, namely Salpeter (1955) and Kroupa (2001), and are provided for two different assumptions regarding the mass loss along the RGB (Section 3.4.2), which result into various HB morphologies. These are indicated in Table 2. In the following subsections we discuss the various model output and their comparisons with observational data and with similar models from the literature.

4.1 Luminosity contributions by stellar phases

Fig. 13 shows the contributions from the various evolutionary phases to the total bolometric, V and K luminosities (from top to bottom) of metal-poor, solar metallicity and metal-rich SSPs, respectively (from left to right).

As in the solar metallicity SSP already discussed in M98, most bolometric energy is shared by the three main phases – MS, TP-AGB and RGB – independent of metallicity (cf. Fig. 4). The energetics of young SSPs ($t \lesssim 0.3$ Gyr) is dominated by MS stars, that of SSPs with $t \gtrsim 2$ Gyr by RGB stars. SSPs with ages in the range $0.3 \lesssim t \lesssim 2$ Gyr are dominated by TP-AGB[6] stars except in the metal-poor stellar population, where AGB, MS and HB have similar

---

relation between [Fe/H] and [Z/H] is: [Fe/H] $=$ [Z/H] $- 0.93([\alpha/\mathrm{Fe}])$ (Thomas & Maraston 2003).

[6] Note that in the figure the total AGB contribution, i.e. that from E-AGB plus TP-AGB, is plotted, but we know from Section 3.1 that the AGB phase is dominated by the TP-AGB
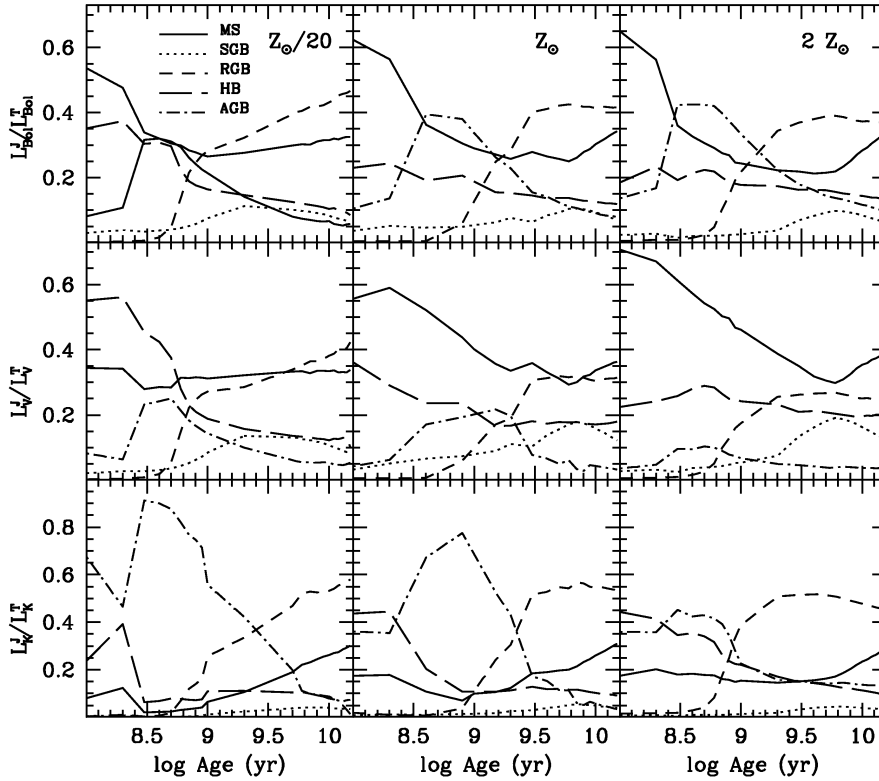
Figure 13. Luminosity contributions in bolometric, *V* and *K* (from top to bottom) of evolutionary phases and their dependences on age and metallicity. From left to right, metal-poor, solar metallicity and metal-rich SSPs (with a Salpeter IMF) are shown. Note that the *y*-scale of the bottom panel is not the same as in the other two panels.

contributions. For ages older than ~6 Gyr, the MS contributions tend to rise. This effect is caused by the MS integrated luminosity decreasing slower than $b(t)$. As the total fuel stays nearly constant, the net result is a lower total luminosity as mainly due to a lower PMS luminosity.

The main contribution to the *V* luminosity comes always from MS stars, except for the metal-poor SSP, where at young ages the HB phase has a relatively larger contribution, and at very old ages the RGB is the dominant phase for the *V*-luminosity, which is due to the warm RGB temperatures at such low metallicity.

Finally, the light in the *K* band [and in the near-infrared (IR) in general] in the age range $0.3 \lesssim t \lesssim 2$ Gyr is dominated by TP-AGB stars at every metallicity, a rôle taken over by the RGB at old ages. These results demonstrate the importance of including the TP-AGB phase for a correct interpretation of rest frame near-IR colours and luminosities of 1 Gyr stellar populations

4.2 Spectral energy distributions with TP-AGB

The synthetic SEDs of old stellar populations, in particular the HB morphology, have been compared with *International Ultraviolet Explorer* data of GCs in Maraston & Thomas (2000) up to the metallicity of 47 Tucanae. In this section we focus on the most relevant features of the new model SEDs, namely the inclusion of the spectra of C- and O-type TP-AGB stars. We will compare the SEDs with a sample of Magellanic Cloud GCs for which data in the whole spectral range from *U* to *K* are available, and with models from the literature. Further comparisons with both observational data and models using broad-band colours and spectral indices will take place in upcoming sections.
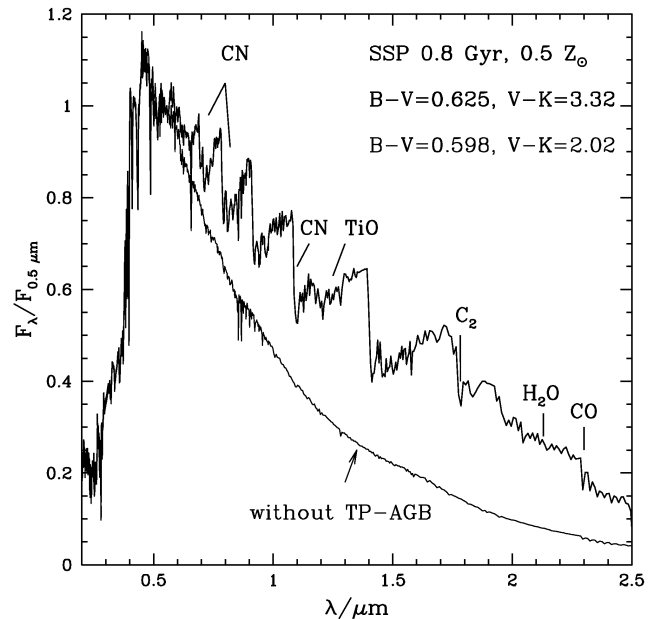

Figure 14. The effect of the TP-AGB phase on the spectral energy distribution of a 0.8 Gyr stellar population with $Z = 0.5\, Z_\odot$ (thick line). The same SSP without the TP-AGB phase is shown as a thin line. The integrated $B - V$ and $V - K$ colours obtained on both SEDs are given. The most important absorption bands typical of C-stars (e.g. C_2, CN), O-stars (e.g. H_2O, TiO), or both (e.g. CO) are indicated. The relative proportions of fuel in C and O stars at this metallicity and age is 9:1 (cf. Fig. 12).
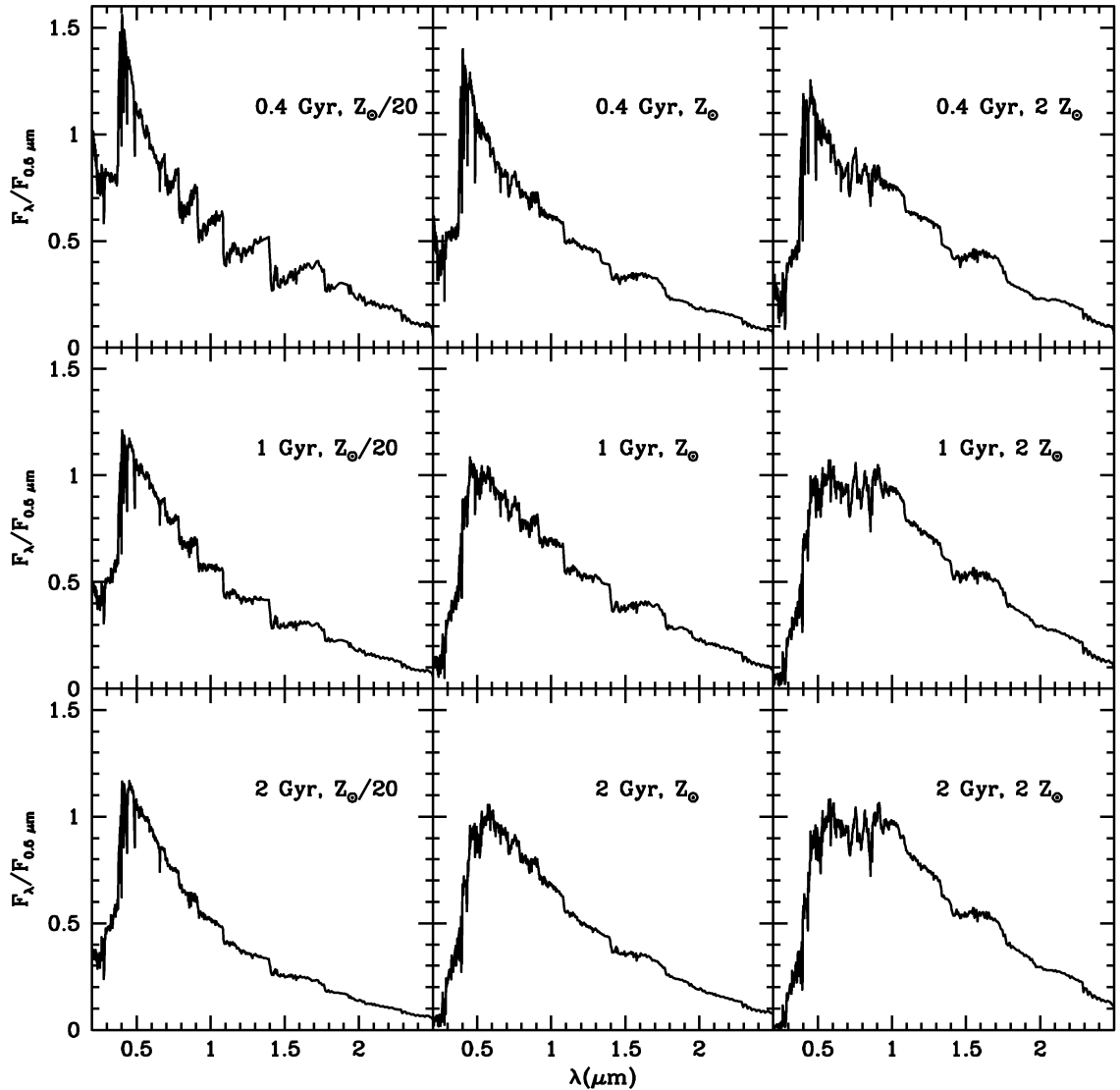
Figure 15. Effect of the metallicity of the TP-AGB stars on the SEDs of 0.4-, 1- and 2-Gyr stellar populations. From left to right, the metallicity increases from $Z_\odot/20$ to $2\,Z_\odot$, and with it the relative importance of oxygen-rich stars over carbon-rich stars.

4.2.1 Fingerprints of ∼1 Gyr populations

The inclusion of the TP-AGB phase in a model SED is substantial at ages in the range $0.3 \lesssim t \lesssim 2$ Gyr where the fuel consumption in this phase is maximum (cf. Section 3.1.3). This is shown in Fig. 14, where two model SEDs of 0.8 Gyr, $0.5\,Z_\odot$ with and without the TP-AGB phase are compared. While the optical part of the spectra is insensitive to the presence of the cool TP-AGB stars, the near-IR part changes dramatically. Not only does the absolute flux in the near-IR region increase by nearly a factor of 3, but also peculiar absorption features appear (e.g. CN, C_2 in C-stars and H_2O and CO in O-stars; see e.g. Lançon & Wood 2000 for more details). These absorption features besides the integrated colours can be used as indicators of ∼ 1-Gyr stellar populations in the integrated spectra of stellar systems. For example, Mouhcine et al. (2002) detected carbon molecules absorptions in the near-IR spectrum of W3, a massive GC of the merger-remnant galaxy NGC 7252 that we previously suggested to be in the AGB phase transition based on its *B*, *V*, *K* colours (Maraston et al. 2001a).

As discussed in Section 3.4.3, the relative proportions of C- and O-stars depend on metallicity, for the model of Fig. 14 the ratio was 9:1. The effect of considering other metallicities is displayed in Fig. 15, where 0.4-, 1- and 2-Gyr SSPs with chemical compositions $Z_\odot/20$, $Z_\odot$ and $2\,Z_\odot$, are shown. The larger total metallicity favours the production of O-rich stars over that of C-rich stars. This is evident in the integrated SEDs as the disappearing of the CN and C_2 bandheads at $1 \lesssim \lambda\,(\mu m) \lesssim 1.5$ typical of C-stars in favour of the H_2O molecules around 1.6 µm. Several line indices are defined that trace these spectral features (e.g. Aaronson, Frogel & Persson 1978; Frogel et al. 1978; Alvarez et al. 2000) and can be used in extragalactic studies. With the new spectra we are in the position of computing the integrated indices for the SSP models (see also Lançon et al. 1999).

Fig. 16 shows three of these indices. The C_2 index (Alvarez et al. 2000) measures the strength of the bandhead at 1.77 µm (Ballik & Ramsay 1963) and is defined as the ratio between the fluxes in the regions 1.768–1.782 µm and 1.752–1.762 µm. The water
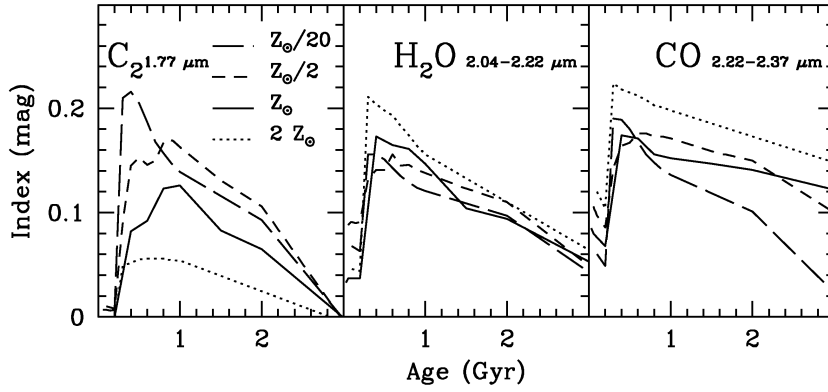
Figure 16. The IR indices C_2, H_2O and CO and their dependence on age and metallicity. The defining wavelengths are indicated, indices are expressed in magnitudes.
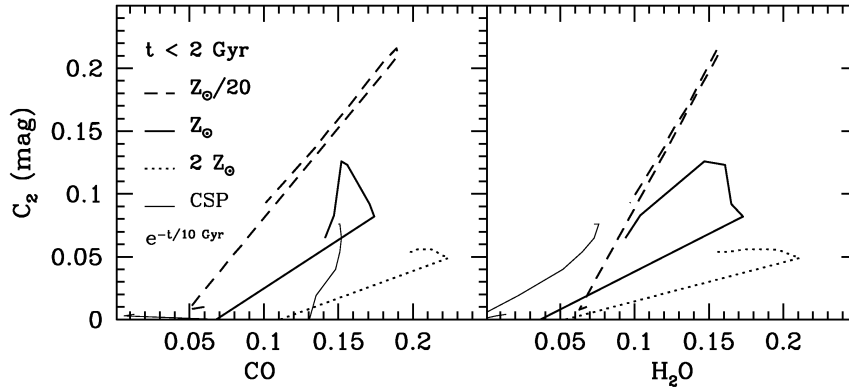
Figure 17. Diagnostic index-index diagrams C_2 versus CO (left-hand panel) and C_2 versus H_2O (right-hand panel), for stellar populations younger than 2 Gyr. The thick lines are SSPs with various metallicities, the thin line shows the effect of an extended exponentially declining star formation history, SFR $\propto$ $e^{-t/\tau}$, with $\tau = 10$ Gyr.

vapour absorption band index H_2O measures the ratio of the flux densities at 2.04 and 2.22 μm, based on the *Hubble Space Telescope* *(HST)*/NICMOS filters F204M and F222M, or at 1.71 and 1.80 μm, based on the *HST*/NICMOS filters F171M and F180M, and the CO index the flux densities at 2.37 and 2.22 μm, based on *HST*/NICMOS filters F237M and F222M. The indices are defined in magnitudes and normalized to Vega.[7]

The C_2 index is a strong function not only of the age, peaking at the time of the AGB phase transition, but especially of the chemical composition, its value decreasing with increasing metallicity, following the decrease of the fuel in C-stars. The water vapour is rather insensitive to the chemical composition, hence is a good age indicator for ages between 0.4 and 2 Gyr. The CO index behaves similarly to the H_2O.

The combination of indices that works best to unveil the presence of $\sim$1 Gyr stellar populations and their chemical composition is C_2 together with H_2O, as shown in Fig. 17. In fact this diagram not only splits very nicely the metallicity effects, but also separates instantaneous bursts (SSPs, thick lines) from stellar populations formed with extended star formation, as shown by the thin line for an exponentially declining star formation history, SFR $\propto$ $e^{-t/\tau}$ with $\tau = 10$ Gyr.
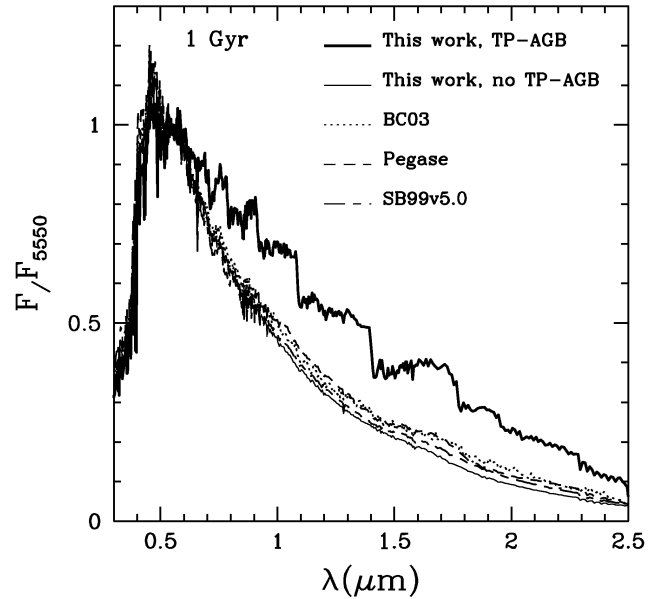
Figure 18. Comparison of the 1 Gyr, solar-metallicity SED of this paper (thick line) with other models from the literature, from Bruzual & Charlot (2003, dotted line), from the PEGASE code (PEGASE.2, dashed line) and from the latest version of Starburst99 (Vázques & Leitherer 2005, long-dashed-short-dashed line). Our SED without TP-AGB phase is shown as a thin solid line.
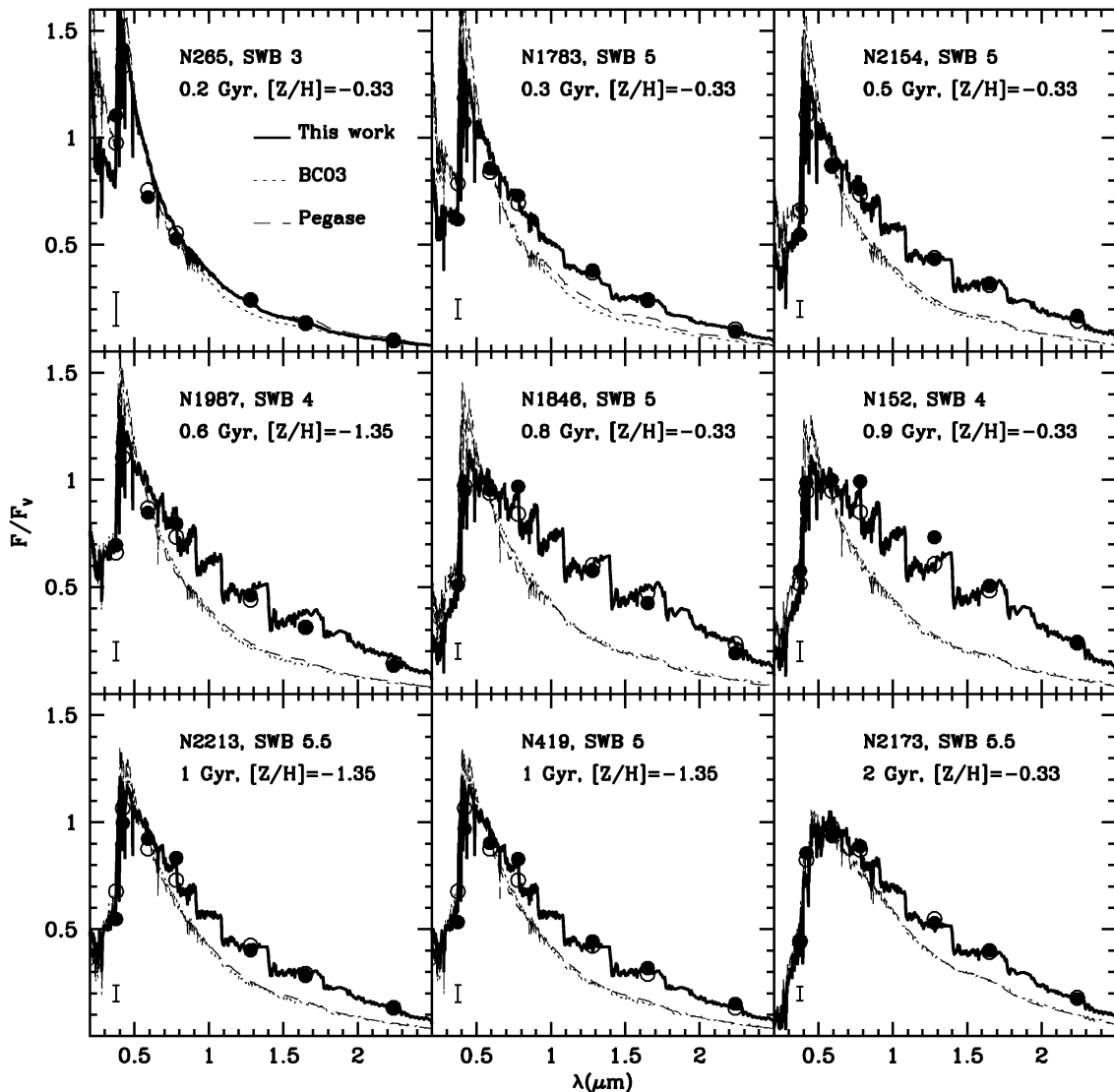
[7] Using a spectrum of Vega taken with *HST* and kindly provided by Bender, the zeropoints are: $C_2 = 0.038$; $H_2O_{1.71\ \mu m} = 0.160$; $H_2O_{2\ \mu m} = -0.360$; CO $= 0.263$, that have to be subtracted to the indices.

Figure 19. SED fitting of MC GCs data (filled points). In each panel the cluster ID and SWB type (the latter from Frogel et al. 1990) are indicated. Sources of data are: van den Bergh 1981 for U, B, V; Persson et al. (1983) for J, H, K; Goudfrooij et al. (in preparation) for V, R, I. The reddening $E(B - V)$ is taken either from Persson et al. (1983) or from Schlegel, Finkbeiner & Davis (1998). The largest error (on the flux in the B band) is shown. Lines show ours, the BC03 and the PEGASE.2 models (solid thick, and dotted and dashed thin lines, respectively) and the ages/metallicities of the fits. For our models also the broad-band fluxes are given (empty circles).

4.2.2 Comparison with literature and data

Fig. 18 shows our SED of a 1 Gyr, $Z = Z_\odot$ SSP (thick line) and similar models from Bruzual & Charlot (2003, hereafter BC03), from the PEGASE code (Fioc & Rocca-Volmerange 1997, version 2 as available at http://www.iap.fr/pegase, hereafter PEGASE.2 models) and from the latest version of STARBURST99 (Vázques & Leitherer (2005), long-dashed-short-dashed line). BC03, PEGASE.2 and STAR-BURST99 are very similar to each other, which is due to their use of the Padova tracks, and are more consistent with the version of our models that do not include the TP-AGB phase than with the version in which the TP-AGB is accounted for. This result is not easy to understand. In the BC03 models the inclusion of C-stars is accounted for by means of unpublished theoretical spectra and an unspecified temperature–luminosity relation, therefore it is hard to make a meaningful comparison with our models. In the PEGASE.2 models and in the latest version of the STARBURST99 models, the TP-AGB phase is included by adopting theoretical prescriptions for luminosities and lifetimes (Gronewegen & de Jong 1993; Vassiliadis & Wood 1993, respectively), but the key information concerning the TP-AGB fuel consumption as a function of mass, its comparison with the Frogel, Mould & Blanco data, the inclusion of carbon stars and which spectra are assigned to TP-AGB stars are not specified.

We now compare the model SEDs with Magellanic Cloud GCs, which are the ideal templates in the age range relevant to the TP-AGB. In M98 we used the data available at the time, namely U, B, V, K. Here we complete the wavelength coverage by adding data in the R and I_C bands from new observations of a sample of MC GCs in the relevant age range (Goudfrooij et al., in preparation). For this sample we can perform the SED fittings. These are shown in Fig. 19, in which nine out of the 20 objects of the Goudfrooij et al. (in preparation) sample are considered, according to the availability of all bands and also for reasons of space, since some

objects display basically the same SEDs. The selected GCs span the interesting range in SWB (Searle, Wilkinson & Bagnuolo 1980) types from 3 to 5.5. The SWB scheme is a ranking of the MC GCs in terms of age/metallicity, the selected types referring to the age range $0.1 \lesssim t \lesssim 2$ Gyr that is relevant to the model comparison. GCs with greater types are older and more metal-poor. The type 7, for example, corresponds to Milky Way like objects, with ages ~ 13 Gyr and [Z/H] ~ -2. As discussed by Frogel et al. (1990) the exact ranking of some individual clusters might be not so meaningful, but the range from 4 to 5.5 corresponds to objects with the largest numbers of AGB stars, which are the only ones in which carbon stars are detected (see fig. 3 in M98). Therefore, the GCs in this SWB range span average ages between ~ 0.3 and ~ 2 Gyr (cf. table 3 in Frogel et al. 1990). Indeed, ages determined by various methods agree generally well with the SWB ranking. For example, in order to fit NGC 1987 we use an SSP with the age and the metallicity as determined in the literature (from Girardi et al. 1995; Ferraro et al. 1995), and the result is very good. However, we emphasize that with the exercise of Fig. 19 we do not aim at deriving precise ages for the objects, but rather at illustrating the effect of the TP-AGB phase. Fig. 19 shows that their SEDs can be fitted only with a proper inclusion of the TP-AGB energy contributions and the spectra of C- and O-stars.

The SSPs have metallicities either half-solar or $1/20$ Z$_{\odot}$ (i.e. [Z/H] $= -0.33$ and [Z/H] $= -1.35$), with thick lines showing our models, and dotted and dashed thin lines those by BC03 and PEGASE.2, respectively. For the latter the lower metallicity is [Z/H] ~ -0.7. For our models we show also the broad-band fluxes (empty circles). Each panel presents an individual GC SED (filled points). Starting from the top left, object NGC 265 with SWB $= 3$ is a pre-AGB GC whose SED does not yet display evidences of TP-AGB stars redwards the R-band. The situation changes completely when later SWB types are considered and the typical features of the

cool TP-AGB stars appear in the near-IR spectrum. Their *complete* SEDs are well fit by our models.

The models of BC03 and PEGASE.2 do not reproduce the observed SEDs with the same SSP parameters, displaying substantially less flux redward of the R-band. The same comparison holds for the STAR-BURST99 models (not shown, see Fig. 18). The obvious conclusion is that the recipes for the TP-AGB adopted in those models are not adequate at describing real stellar populations with TP-AGB stars. Further discussions on these models is found in the next section. There is no combination of age and metallicity that allows one to fit the high fluxes both blueward and redward of the V band unless the TP-AGB phase is included as shown by the thick solid lines. As we will see in Section 6, in case of galaxies a composite stellar population in which a late burst is superimposed to an old component can fulfil the need for high fluxes both in the blue and near-IR (relative to V). This option is clearly not viable in case of GCs.

In the next section we will show the comparison with more objects by means of broad-band colours.

4.3 Broad-band colours

Broad-band colours are computed for several filter systems (e.g. Johnson–Cousins, Sloan, *HST*). In the following subsections we will compare them with Magellanic Cloud GCs and Milky Way halo and bulge GCs, which allows the check of young and intermediate age models with slightly subsolar metallicities, and old ages for a wide range of metallicities, respectively. Comparisons will be also made with models from the literature.

4.3.1 TP-AGB-dominated $\sim$1-Gyr models

In Fig. 20 we perform a comparison similar to that shown in Fig. 19 by means of broad-band colours, which allows us to use a larger
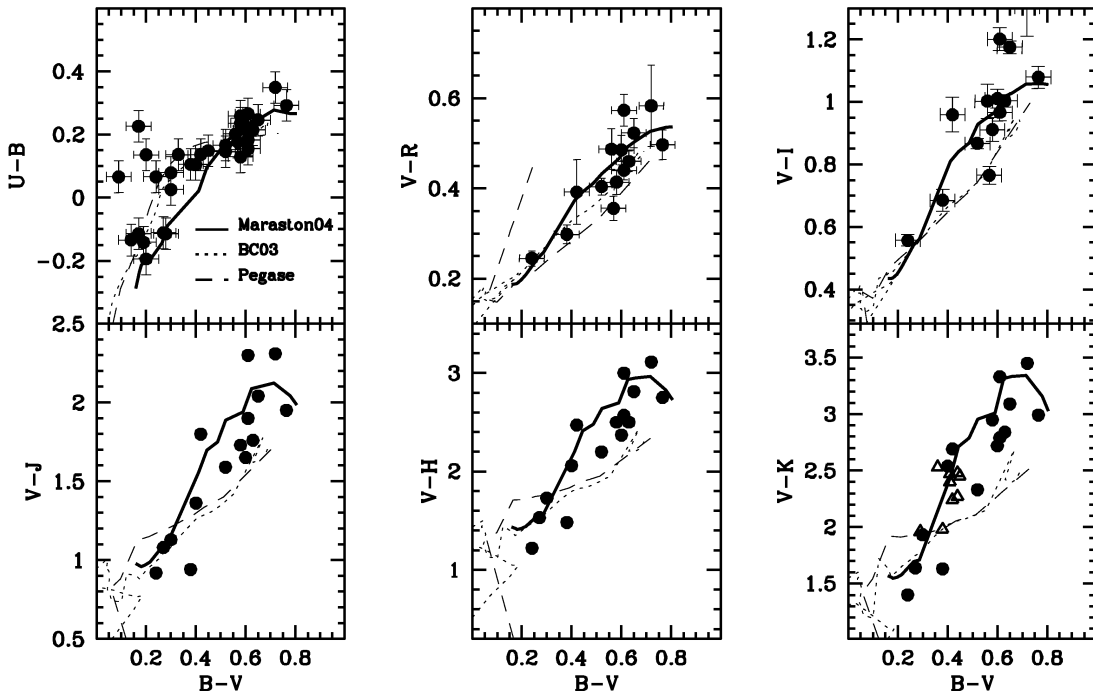

Figure 20. Calibration of TP-AGB-dominated synthetic broad-band colours with data of MC GCs (filled circles). MC data are selected to belong to SWB types between 3 to 6, appropriate to the age range and the metallicity of the models (sources of data as in Fig. 19). Open triangles show the star clusters of the merger remnant galaxy NGC 7252 (*V* photometry from Miller et al. 1997, *K* photometry from Maraston et al. 2001a). Models have ages lower than 2 Gyr and metallicities 0.5 Z$_{\odot}$, with solid, dotted and dashed lines referring to this work, BC03 and PEGASE.2.

data sample. We also include the data of the GCs in the merger remnant galaxy NGC 7252 (Maraston et al. 2001a, open triangles). The models are selected to have ages smaller than 2 Gyr and half-solar metallicity.

The AGB phase transition among the clusters appears as an enhancement of the IR luminosity with respect to the optical one, that increases with increasing wavelength, with e.g. the $V - K$ colour reaching values larger than 3. All bands redwards of R are affected. The models of this paper provide a good description of TP-AGB-dominated stellar populations in a large wavelength range. As already shown in Maraston et al. (2001a), the models reproduce very well also the integrated colours of the young GCs of the merger remnant galaxy NGC 7252.

The other models considered here, namely those by BC03 and PEGASE.2[8] do not exhibit the 'jump' in the near-IR colours displayed by the MC GCs, remaining systematically bluer than the data and evolving slowly towards the red colours produced by the rise of the RGB phase at $t \gtrsim 1$ Gyr. This pattern is equivalent to the SED comparison discussed in the previous section, again suggesting that the TP-AGB phase is not fully accounted for in these models.

BC03 argue that stochastical fluctuations in the number of TP-AGB stars suffice to explain the full range of observed $V - K$ colours of MC GCs. These effects are mimicked by means of a stochastic IMF in a $\sim 2 \times 10^4 \, M_\odot$ model star cluster.

From their fig. 8 one sees that the simulations match the colours of the youngest MC GCs, whose near-IR light is dominated by red supergiants with lifetimes $\sim 10^6$ yr, very well. The TP-AGB phase instead lasts 10 times longer and is therefore less affected by stochastical fluctuations. As a consequence the simulations are less successful in covering the observed colours of the TP-AGB-dominated MC star clusters. Moreover, the probability distributions of the points in their simulations is skewed towards bluer colours. This implies that it would be highly unlikely to observe a GC on the red side of the models if stochastical fluctuations were dominating the distribution of the data. Instead the data scatter exactly to the red side of the models.

A further important point is that the importance of stochastical fluctuations depends dramatically on the mass of the GC. While the effect is relatively large for masses of the order $10^4 \, M_\odot$ (considered in the BC03 simulations), it is significantly smaller at $10^5 \, M_\odot$ and completely negligible around $10^6 \, M_\odot$. Hence, the stochastical fluctuations, based on a $10^4 \, M_\odot$ cluster, are not appropriate to describe the colours of the star clusters of the merger-remnant galaxy NGC 7252 (shown as open triangles in Fig. 20). Their luminous masses are estimated to be at least $10^6 \, M_\odot$ (Schweizer & Seitzer 1998) ranging up to even $\sim 10^8 \, M_\odot$ as confirmed dynamically for the most luminous object (Maraston et al. 2004). The expected stochastical fluctuations for such very massive objects are of the order of a few per cent (Maraston et al. 2001a) and their colours are not explained by the BC03 models without fluctuations (Fig. 20). Instead, their colours are nicely explained by a TP-AGB phase such as in the MC clusters (Maraston et al. 2001a and Fig. 20), a conclusion that is supported by the direct observa-

tion of carbon stars in their spectra (Mouhcine et al. 2002 with SOFI observations).

To conclude, while we fully agree that stochastical fluctuations in the number of stars along *short* evolutionary phases[9] scatter the near-IR colours of small-mass star clusters, the account of these effects should be considered on top of the stellar evolutionary phases. For example it seems more likely to us that the lack of the AGB phase transition in the BC03 models comes from the fact that the TP-AGB bolometric contribution never exceeds ~ 10 per cent (fig. 4 in Charlot & Bruzual 1991). This is at variance with the measured bolometric contribution of the TP-AGB phase (~ 40 per cent, fig. 3 in M98) which was evaluated by taking stochastical fluctuations into account.

In the PEGASE.2 models the details of the inclusion of the TP-AGB phase are not specified. However, from Fig. 2 in Fioc & Rocca-Volmerange (1997) one sees that a jump in $V - K$ of ~ 0.6 mag (up to $V - K \sim 2.2$) occurs at $t \sim 0.1$ Gyr, after which the evolution of this colour is nearly constant. The AGB phase-transition as exhibited by the MC star clusters does not take place in their models.

4.3.2 Age and metallicity relations of old models

Milky Way GCs spanning a wide range of metallicities at nearly the same age are ideal to calibrate the synthetic colours/metallicity relations. Fig. 21 shows a comprehensive comparison of old (13 Gyr) models with all available photometry of Milky Way GCs. Data are plotted towards the [Fe/H] parameter of the Zinn & West (1984) scale, that we show to reflect total metallicities (Thomas, Maraston & Bender 2003a). Data for the two metal-rich GCs of the galactic bulge NGC 6528 and NGC 6553 are the open triangles. Models are shown for both the Kroupa and the Salpeter IMF (solid and dashed lines, respectively) only for completeness since we found that the optical colours of SSPs are virtually unaffected by plausible IMF variations (M98). The dotted line shows the BC03 models for the same age and the Salpeter IMF.

The match between models and data is very good, except for the $B - V$ colour, which appears to be systematically redder in the models (of 0.05 mag). We have checked that this feature is common to all SSP models considered in the paper, namely the BC03, PEGASE.2, Worthey (1994) and Vazdekis et al. (1996), and was discussed by Worthey (1994) and Charlot et al. (1996). We now investigate the origin of the offset.

The offset cannot be attributed to HB morphologies. The blue HB morphology[10] of most GCs with metallicities below -1.3 is already accounted for in our models at 13 Gyr and $[Z/H] = -2.25$ (cf. Fig. 11). At 13 Gyr and $[Z/H] = -1.35$ the HB morphology is intermediate (cf. Fig. 11). A purely blue HB, with $T_{\rm eff}$ up to 10^4 K would make the $B - V$ bluer by 0.03 mag. However, the GCs with metallicities $\gtrsim -1$. have a red HB and still their $B - V$ is bluer than the models. The latter data can be better matched with a younger age, e.g. 8 Gyr, which is perhaps not excluded (e.g. Rosenberg et al. 1999). However, this younger age worsens the fit to $U - V$ and $U - B$.

A more likely explanation is a defect in the colour–temperature transformations. This issue is extensively addressed by Vanden-Berg & Clem (2003), who provide a set of transformations to cure the $B - V$ problem, which is attributed to deficiencies of the model atmospheres. We have found that the $B - V$ colours in their

---

[8] For this comparison we focus on those models for which the TP-AGB is stated to be included. The Worthey (1994), the Vazdekis et al. and the STARBURST99 (Leitherer et al. 1999) models do not treat the TP-AGB phase. Mouhcine & Lançon (2002) include the TP-AGB phase in such a way as to reproduce the $B - V$ vs. $V - K$ synthetic diagram published by Maraston et al. (2001a). However, the TP-AGB bolometric contribution in their models is up to 20 per cent (Mouhcine & Lançon 2002), smaller than the observed ~ 40 per cent one (Frogel et al. 1990) reproduced by our models (Fig. 13).

[9] For example the supergiant phase in stellar populations younger than 0.1 Gyr.

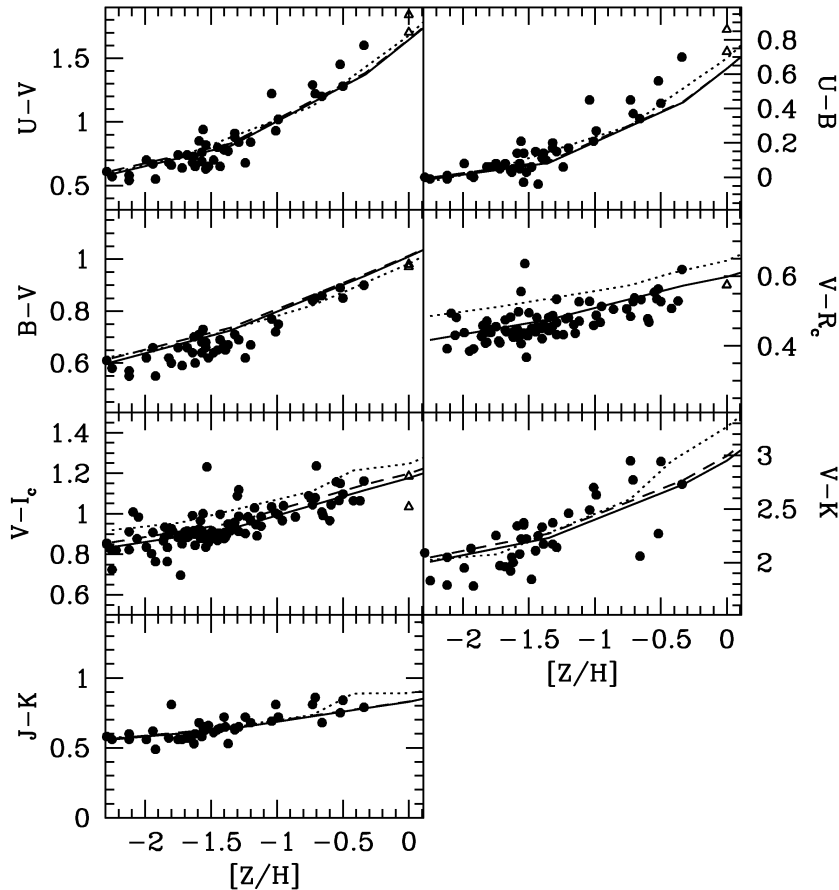[10] As derived from the HBR parameter listed in the Harris (1996).

Figure 21. Comparisons of synthetic broad-band colours with data of Milky Way GCs (as compiled in the Harris – 1996 and revisions – catalogue). The data of the $\sim Z_\odot$ bulge GCs NGC 6528 and NGC 6553 are shown as open triangles. Reddening has been subtracted as in Barmby & Huchra (2000). Metallicities are on the Zinn & West (1984) scale. Solid lines show SSP models of age 13 Gyr, Kroupa IMF, and blue/intermediate HB morphology at $[Z/H] \lesssim -1$. The same models with a Salpeter IMF are shown as dashed lines. The dotted lines are the BC03 models for the same age.

transformations are very close to those of the BaSel library for the turnoff temperatures of the 13-Gyr models ($5800 \lesssim T_{\rm eff} \lesssim 6700$ K, $\log g \sim 4.5$), but are *bluer* for the RGB base ($4900 \lesssim T_{\rm eff} \lesssim 5300$ K, $\log g \sim 3$), by 0.1 mag at $[Z/H] \sim -2.25; -1.35$. Since the RGB contributes ~ 40 per cent to the V luminosity at $[Z/H] = -1.35$ and below (cf. Fig. 13), the use of the VandenBerg & Clem (2003) transformations would be able to reduce significantly the discrepancy between data and models. It is intriguing, however, that the Vazdekis et al. models that adopt an empirical temperature–colour relation instead of the theoretical one suffer from the same problem. Also, Bruzual & Charlot (2003) compare the integrated $B - V$ of solar metallicity SSPs based on the BaSel and the Pickles empirical library, and found negligible differences. Though their exercise refers to solar metallicity, while our comparison focuses on subsolar chemical compositions, it has to be expected that if a fundamental problem in the treatment of the opacity would be responsible for the colour offset, this would be even more serious at higher metallicities.

We are left with one alternative explanation, that is an offset in the photometric bands, due to the broad-band filters. Indeed, two different B filters are used, the so-called B2 and B3 (Buser, private communication), in order to compute $U - B$ and $B - V$, respectively. These are commonly defined as 'standard Johnson B'. The colour $U - V$ is then evaluated by adding $U - B$ and $B - V$.[11] It is hard to trace back which exact filter was used for the data,

[11] We acknowledge a discussion with Buser, who confirmed this fact to us.

therefore we vary the B-filter in the models. The result is that if we use the B2 filter to compute the $B - V$ colour, the latter gets *bluer* by 0.03 mag., again in the direction of improving the comparison, while leaving the $U - V$ colour almost unchanged.

To conclude, either a defect of the model atmospheres, a filter mismatch or a combination of both are the most plausible sources of the discrepancy between data and models in $B - V$. However, since at redshift >0 one needs the whole SED, the use of spectral libraries such as the BaSel one is unavoidable. Instead, in comparing the models with observed colours, it is safer to take the offset of 0.05 mag. into account.

Back to Fig. 21, we see that the BC03 models behave very similarly to ours, with the exception of the $V - R$ and $V - I$ colours, which in the BC03 models appear to be too red when compared to our models and to the data. Reducing the age does not improve the comparison. We cannot explain the reasons for this offset.

4.4 Mass-to-light ratios

The stellar mass-to-light ratios M^*/L are computed as in M98, by taking the stellar mass losses into account. The relation between living stars and remnants is from Renzini & Ciotti (1993), where the remnant mass as a function of the initial mass is given for three types of stellar remnants, i.e. white dwarfs, neutron stars and black holes. These relations are used for every metallicity, the dependence
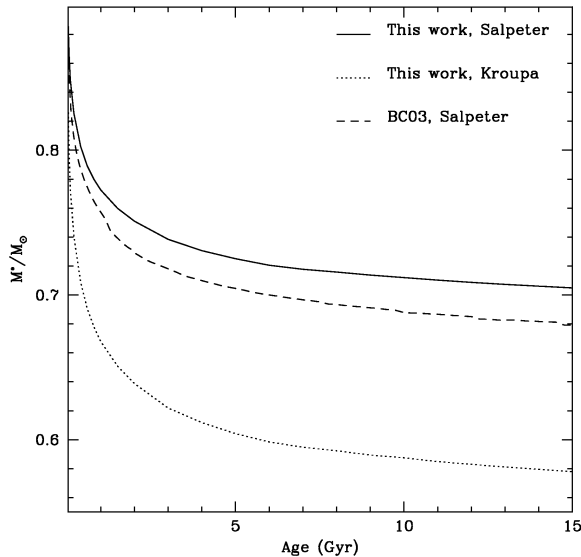
Figure 22. The total stellar mass (normalized to $1\,M_\odot$) of an evolving stellar populations in which the stellar mass losses are taken into account.
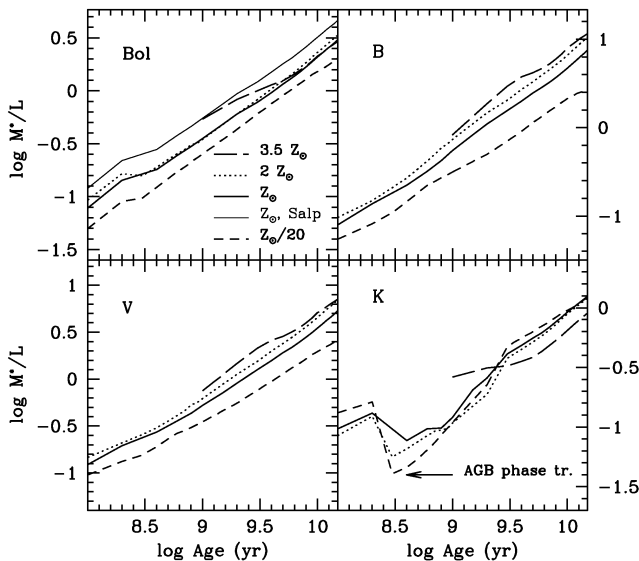

Figure 24. Comparison between model M/L in various bands from different authors (see Footnote 12). All SSPs have solar metallicity and Salpeter IMF.

Figure 23. The dependence of the M^*/L (in solar units) on age and metallicity. Models refer to the Kroupa IMF, for the bolometric the solar-metallicity models for a Salpeter IMF are shown as thin solid line. Note that the 3.5-$Z_\odot$ SSP is computed with the Padova tracks and does not contain the TP-AGB phase.

on the chemical composition entering through the turnoff mass. Fig. 22 shows the stellar mass of an evolving stellar population with an initial mass of $1\,M_\odot$, solar metallicity and Salpeter or Kroupa IMFs (solid and dotted line, respectively). In the case of a Salpeter IMF the stellar mass decreases by ∼30 per cent in 15 Gyr, ∼23 per cent being lost in the first Gyr. The Kroupa IMF with less power in low-mass stars has ∼16 per cent less mass, and correspondingly lower values of M^*/L. The stellar mass of the BC03 models is smaller than that computed in our models.

The basic dependences of the M^*/L's on the SSP parameters, ages, metallicities and the IMF are shown in Fig. 23. The M^*/L's increase with age because the luminosities decrease, an effect independent of the photometric band. An important exception is the
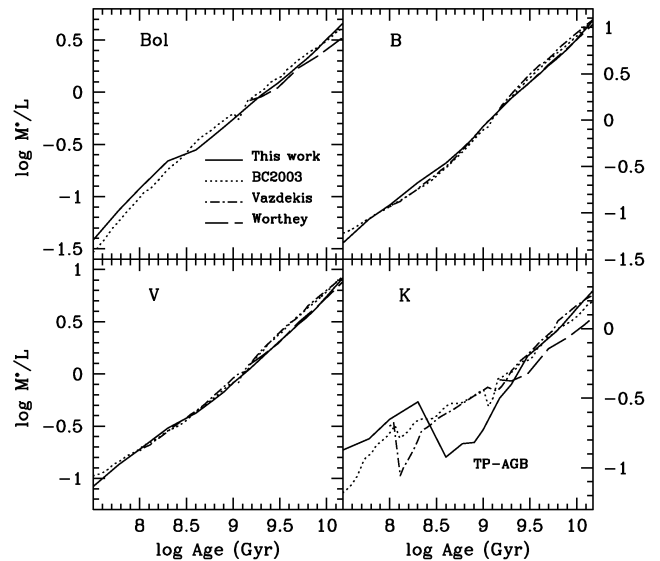
occurrence of the AGB phase transition during which the near-IR luminosity increases with age and therefore the $M^*/L_{\rm near-IR}$ *decreases*, by a factor 3–5 with respect to models not including the TP-AGB phase.

Metallicity effects are strongly dependent on λ. The values of M^*/L generally increase with increasing metallicity because the luminosities decrease (which is explained by lower MS and PMS luminosities with increasing metal content, Section 3.1). However, in the near-IR, a transition occurs at $\lambda \gtrsim I$-band and the values of M^*/L become *independent* of metallicity at ages $\gtrsim 2$ Gyr. The reason for this is that a high-Z SSP produces less light than one with a lower amount of metals, but most of the energy is emitted preferentially at longer wavelengths because of the cooler stellar temperatures. Note however that the effect holds until the metallicity is not too large. The very metal-rich SSP of our set ($Z = 3.5\,Z_\odot$) has $M^*/L_{\rm near-IR}$ smaller than the others SSPs.

The effect of the IMF was amply discussed in M98. The main result was that the M^*/L of SSPs is minimal for Salpeter and increases for both a flattening or a steepening of the IMF. The reason is that a larger amount of mass in massive remnants or in living stars is present. This interesting point stems from considering the evolution of the stellar mass. The models in Fig. 23 refer to a Kroupa IMF; the effect of having a Salpeter IMF is shown only in the bolometric (solid thin line), with the M^*/L being larger by a factor ∼1.5. A similar scaling factor is found at the various values of λ, almost independent of metallicity.

Finally, our models are compared with others in the literature in Fig. 24.[12] The models by BC03 have a bolometric M/L that is larger than ours around ages of a few Gyr, because the luminosity of the Padova tracks is smaller due to the delayed development of the RGB phase (Fig. 7). The effect is partly counterbalanced by a slightly smaller stellar mass (Fig. 22). The largest differences are found in the near-IR. The M/L_K of the BC03 models is higher than

---

[12] During the referee process of this paper A. Vazdekis provided us with a new version of his model *M/L* in which the values have been revised. This explains why Fig. 24 in its final version differs from that of the astro-ph submitted paper.
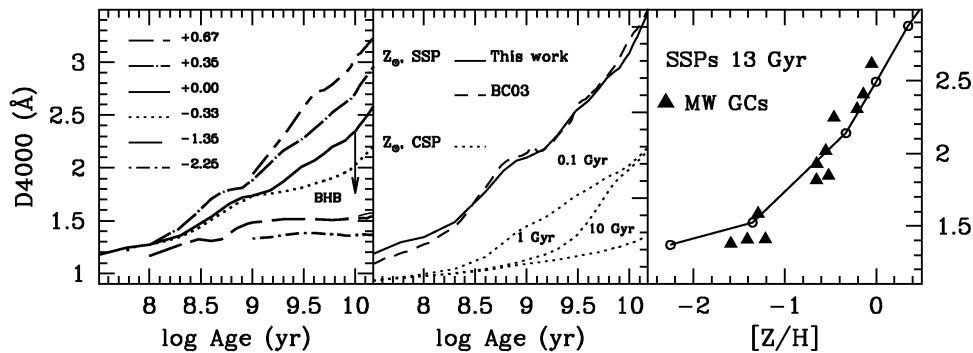
Figure 25. The D-4000 break all at once. Left-hand panel: the dependence on age, metallicity and horizontal branch (HB). The two lowest metallicity SSPs are shown with both blue and red HBs (thick and thin lines, respectively), and a negligible impact is found. The arrow points to the value of the break when a blue HB is considered in the 10 Gyr, solar metallicity SSP. A sizable decrease of ~ 0.6 Å occurs as a consequence of a blue instead of a red HB. Central panel: the dependence of the D-4000 break on the input stellar tracks, shown using the BC03 models and solar metallicity SSPs, is negligible. The dependence on the star formation history is highlighted by means of composite stellar population models with various exponentially decreasing star formations (dotted lines, the e-folding times are labelled beside each curve). Right-hand panel: comparison of the synthetic D-4000 break of SSPs with various metallicities and the constant age of 13 Gyr with GC data.

ours around 0.8–1 Gyr due to the lower contribution of the TP-AGB in their models. At old ages it is instead smaller, due to the cooler RGBs of the Padova tracks (cf. Fig. 9). The models by Worthey (1994) have smaller $M/L_{\rm bol}$ and $M/L_{\rm K}$, due to larger bolometric and near-IR luminosities. This is possibly due to a larger number of upper RGB stars with respect to that predicted by the Padova isochrones (Charlot et al. 1996). Note also that the Worthey (1994) values of M/L do not take the stellar mass losses into account. Finally, the models by Vazdekis et al. (1996) behave in general similarly to the BC03 ones, which is due to the use of the Padova tracks in both models. Some differences appear in the K band, however. At $t \sim 10^8$ yr a dip in the Vazdekis models is present that is not found in the BC03 models, therefore it can hardly be connected to the Padova tracks, unless the two models adopt a different releases.

4.5 Lick indices

The Lick indices of SSP models computed by means of the Lick fitting functions (Worthey et al. 1994) have solar-scaled element abundance ratios at high-metallicities $[Z/H] \gtrsim 0.5\,Z_{\odot}$ (Worthey et al. 1994; Maraston et al. 2003). Therefore, they are not adequate to model stellar systems with high-metallicities and enhanced $\alpha/{\rm Fe}$ abundance ratios, such as bulge GCs, elliptical galaxies and bulges of spirals (Maraston et al. 2003). At low metallicities, these models trace element-abundance ratios that are proper to the stars used to compute the fitting functions, which are a mix of solar-scaled and enhanced ratios (Maraston et al. 2003; Thomas et al. 2003a). Finally, the models do not contain the explicit dependence on the relative elemental proportions, which is instead a powerful tool to constrain the star formation history of stellar systems (Matteucci 1994; Thomas, Greggio & Bender 1999).

To circumvent the limitations quoted above, we have computed new-generation stellar population models of Lick indices that include the dependence of the element ratios. The models allow several non-standard elemental mixtures, and are checked to reproduce the Lick indices of Milky Way halo and bulge GCs for their proper element ratios. The models of the classical Lick indices are in Thomas et al. (2003a) and those of the high-order Balmer lines in Thomas et al. (2004).

4.6 The D-4000

The D-4000 break is computed adopting the definition of Bruzual (1983). The main features of this index have been outlined by several authors (among others Bruzual 1983; Barbaro & Poggianti 1997; Gorgas et al. 1999) and will not be repeated here. What we add are two interesting behaviours.

Fig. 25 summarizes the main features of the D-4000 break. Typically used as pure age indicators, the D-4000 is very much sensitive to metallicity (Fig. 25, left-hand panel), and at low metallicity is actually completely insensitive to age. Interestingly the D-4000, unlike the Balmer lines (Maraston & Thomas 2000) is *insensitive* to the morphology of the HB at low metallicity. This suggests its use as metallicity indicator for low-metallicity extragalactic GCs, as at low metallicity the break is also completely insensitive to age. In contrast we find the break to be very sensitive to blue HB at high metallicity. This is also shown in Fig. 25, in the left-hand panel, where the arrow indicates the value of the break of a 10 Gyr, solar metallicity model with a BHB (see Section 4.8). The D-4000 break is diminished by ~ 0.6 Å. The break is completely insensitive to the IMF, when modified from Salpeter and Kroupa (Fig. 25, central panel), which is obvious because the blue spectral region is not sensitive to the percentage of stars with masses lower than $\sim 0.5\,{\rm M_{\odot}}$.

The presence of several metallic lines in the wavelength windows defining the D-4000 break makes this index possibly dependent on the details of the chemical abundance pattern. Such an effect is likely to occur at metallicities larger than solar, since the solar-scaled models and the $[\alpha/{\rm Fe}]$-enhanced GCs data agree up to solar metallicity (Fig. 25, right-hand panel). This issue is investigated in detail in a forthcoming paper.

4.7 The Ca II triplet index

The equivalent width of the triplet absorption line of calcium at 8600 Å (Ca II) is computed adopting the index definition by Cenarro et al. (2001a). The index CaT* is given by CaT* = CaT$-$0.93PaT, therefore it is decontaminated from the possible contribution by the adjacent Paschen lines (described by means of the index PaT). The integrated indices of the SSPs are computed by adopting the index calibrations with Milky Way stars (so-called fitting functions)
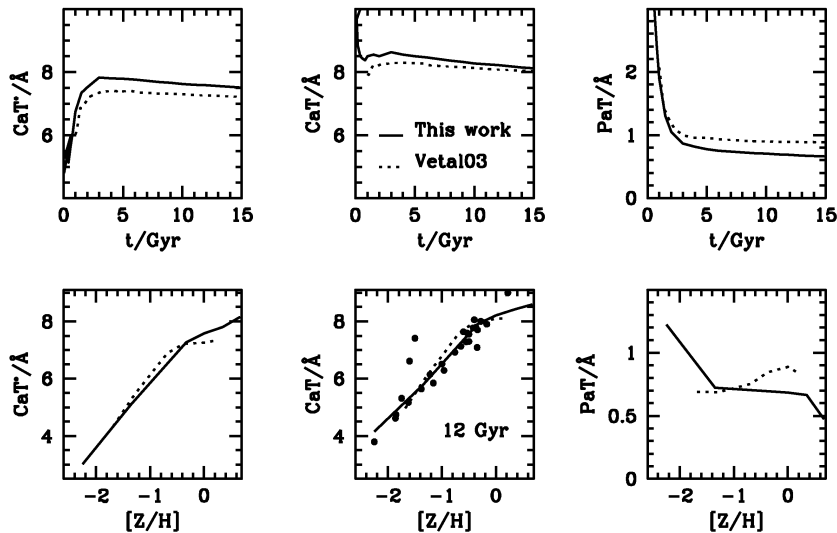
Figure 26. The dependence of the indices CaT*, CaT and PaT on age at fixed solar metallicity (upper row), and on metallicity at the fixed age of 12 Gyr (lower row). Solid and dotted lines refer to the models of this paper and of Vazdekis et al. (2003), respectively, both for a Salpeter IMF. In the lower central panel the models are compared with Milky Way GC data (from Armandroff & Zinn 1988).

Table 3. Effects of high-Z BHBs on various SSP outputs. Numbers refer to the percentage changes for all entries, but for the higher-order Balmer lines Hδ_A, Hγ_A, Hδ_F, Hγ_F, for which the difference (in Å) between the value relative to a BHB and that relative to a red HB is given.

[Z/H]	L_U	L_B	L_V	L_R	L_I	L_J	L_H	L_K	D4000	CaT*	Mg$_2$	Mgb	$\langle$Fe$\rangle$	Hβ	Hδ_A	Hγ_A	Hδ_F	Hγ_F
−0.33	60	38	−8	−30	−41	−52	−56	−55	−21	−8	−6	−17	−19	77	5	2.9	6.4	3.35
0.00	58	38	5	−8	−15	−24	−26	−26	−25	−3	−7	−15	−13	61	4.8	2.4	5.7	2.9
0.35	70	47	12	−4	−12	−26	−31	−32	−25	−2	−12	−18	−14	73	5.7	2.6	6.3	3.1

by Cenarro et al. (2001b, 2002), following a standard procedure to compute absorption line indices by means of fitting functions. As in the case of the Lick indices, the model CaT also reflects the Ca abundances in Milky Way halo and disc stars by construction.

The dependence of the Ca II index on stellar parameters has been discussed by several authors, among the first by Diaz, Terlevich & Terlevich (1989) till the recent papers by Mollà & Garcia-Vargas (2000) and Vazdekis et al. (2003), and by Schiavon, Barbuy & Bruzual (2000), who computed the Ca II index on model atmospheres. Briefly recalling the index is very sensitive to gravity, being strong (weak) in cool giants (dwarfs), therefore it is classically used to investigate the IMF. The effect of calcium abundance is instead still unexplored. We plan to address this issue in a future paper.

The dependence of the indices on the IMF is discussed in Saglia et al. (2002) and Vazdekis et al. (2003) and will not be repeated here, where instead we focus on age and metallicity. Fig. 26 shows the integrated indices CaT*, CaT, PaT of the SSPs as functions of age for solar metallicity and as functions of metallicity for the fixed age of 12 Gyr (upper and lower rows, respectively). The indices are rather insensitive to age at $t \gtrsim 2$–3 Gyr, which stems from the constancy of the giant component of a stellar population after the RGB phase transition is completed (cf. Fig. 13). The very mild decrease of the indices at high ages is due to the larger contribution of the low-mass MS. Therefore, the effect depends on the assumed IMF, and disappears for IMFs with flat exponents below 0.6 M$_\odot$. In the lower panels we display the strong metallicity dependences of the indices, caused by the fact that CaT measures essentially the RGB population. The saturation of the indices at high Z is most likely

caused by saturation of the Ca II lines at high Z. Finally the central lower panel compares the models with GCs data by Armandroff & Zinn (1988, translated into the Cenarro et al. system by Saglia et al. 2002). The models reproduce well the index–metallicity relation of the Milky Way GCs up to a metallicity of nearly solar.

4.8 Effect of blue HBs at high metallicities

The HB at high metallicity is usually red, however, the presence of exotic blue morphologies cannot be excluded. For example, as already mentioned in Section 3.4.2, two rather metal-rich Milky Way GCs were indeed found to contain 10 per cent of blue HB stars (Rich et al. 1997). Because in extragalactic studies the HB morphology is not directly accessible, it is useful to evaluate theoretically the effect on the SSP models of a BHB at high Z.

Table 3 provides the effects of high Z BHB on various SSP output.[13] The impact is generally expressed as a fractional change, i.e. the percentage variation as referred to the red HB SSP with its sign. For example, at [Z/H] = −0.33, L$_U$ increases by 60 per cent, while L$_K$ decreases by 55 per cent. For the higher-order Balmer lines Hδ_A, Hγ_A, Hδ_F, Hγ_F (Worthey & Ottaviani 1997) whose values cross zero when their strengths decrease, the difference (in Å) between the value with BHB and RHB is given. For example, at

---

[13] In order to evaluate the effect on several other SSP output the readers can compare the models with BHB and RHB that are available at the model web page.

© 2005 RAS, MNRAS **362**, 799–825

the same metallicity, Hδ_A increases by 5 Å when a BHB is present. The obvious consequence of having a blue HB morphology is to enhance the strength of the spectrophotometric indicators in the blue. From this effect comes the age–metallicity degeneracy due to the HB (e.g. Maraston & Thomas 2000), that is, an unresolved BHB in an old stellar population can mimic a substantially younger age. For example, a 10-Gyr SSP with solar metallicity and a BHB would appear as young as 2 Gyr in the Balmer lines. Note that also the metallic indices as well as the D-4000 and the Ca II index change consistently and would yield an age of approximately 2 Gyr. The effect on index–index diagrams is shown in Thomas et al. (2005).

In order to break the age-BHB degeneracy the best strategy appears to be a combination of Balmer lines (or blue colours) and TP-AGB sensitive colours like $H - K$. Indeed as one sees from Table 3 the latter is insensitive to the presence of a BHB while it increases substantially in presence of a real 2 Gyr old population containing TP-AGB stars (Fig. 20).

The values provided in Table 3 allow the evaluation of BHB effects in arbitrary proportions on a stellar population, also when other models from the literature are adopted. In particular, the values in the table can be applied to the models with variable element abundance ratios by Thomas, Maraston & Bender (2003a, for the Lick indices) and by Thomas et al. (2004, for the higher-order Balmer lines).

5 UNCERTAINTIES ON SSPS DUE TO STELLAR TRACKS OR EPS CODES

Two types of uncertainties affect the interpretation of the age and the metallicity of an unresolved stellar population by means of SSPs models. The first group collects what we can call *intrinsic uncertainties*, in the sense that they belong to the physiology of the model. These are led by the 'age–metallicity degeneracy' (e.g. Faber 1972; O'Connell 1980; Worthey 1994; Maraston & Thomas 2000), the effect by which a larger metal content produces similar spectral changes as an older age, and vice versa. To this group belongs the HB morphology and the chemical abundance pattern. These uncertainties cannot be removed, however, they can be taken into account by a proper use of the models.

The other class should be called *transient uncertainties*, in the sense that a solution can be found at some point. To this group belong the discrepancies in the model output that are generated by: (1) stellar evolutionary tracks; (2) transformations to the observables; (3) EPS codes. Charlot et al. (1996) investigated the origin of the discrepancies in their model $B - V$, $V - K$ and M/L_V. Their main conclusions are: (a) the 0.05 mag discrepancy in $B - V$ colour originates from a known limitation of the theoretical spectra; (b) the 0.25 mag discrepancy in $V - K$ comes from the stellar evolution prescriptions; (c) lifetimes and luminosities of post-MS phases are problematic. As different EPS codes were used, their approach did not allow the exploration of the sole effect of stellar models. This is what we shall do here. With the same code we vary the stellar evolutionary input, i.e. the energetics and temperatures matrices, while keeping constant the temperature/colour/spectra-transformation matrix. A similar exercise can be found in Fioc & Rocca-Volmerange (1997), where the impact of varying the stellar tracks from the Padova to the Geneve set is tested. Major differences were found at very young ages (tenths of Myr), that are connected with the recipes of mass loss in massive stars. However, both sets of tracks adopt overshooting, while in the exercise presented here the Frascati tracks do not include this parameter, thereby allowing to

explore its impact on the spectral evolution. In the following we will focus on colours and spectra, since the influence of the stellar tracks on the Lick absorption indices has been discussed by Maraston, Greggio & Thomas (2001b), Maraston et al. (2003). We also leave out the investigation of the uncertainties in the spectral libraries since it is made in BC03.

In Fig. 27 (left-hand panel) we compare selected broad-band colours with solar metallicity and various ages as computed with our code and the Frascati and the Padova stellar tracks (solid thick and thin lines, respectively).

The $V - K$ is the most affected by the stellar models. At $t \gtrsim 2$ Gyr the value obtained with the Padova tracks is redder by 0.08 mag than that obtained with the Frascati tracks. This was expected because the largest difference between the two sets of tracks is the RGB temperature (Fig. 9). The difference is not dramatic because the tracks deviate especially towards the tip, where the evolutionary time-scale is faster, therefore the fuel consumption smaller. Similar values are found at twice solar metallicity.

The $V - I$ is rather insensitive to the choice of the tracks,[14] while the $B - V$ relative to the Padova tracks is bluer at the ages at which the overshooting is important, in agreement with the higher MS luminosity of the Padova tracks (Fig. 7). At old ages the two model $B - V$ are in perfect agreement. As for the metallicity scale (right-hand panels), the largest discrepancies are found when the colours involving near-IR bands are considered, which again stems from the different RGB temperatures. For example, at low metallicities the Padova tracks are hotter than the Frascati ones, and the relative colours bluer. Therefore, an observed colour (at given age) is interpreted as connected to a higher metallicity (e.g. a $V - K$ of 2 requires [Z/H] ~ -1.7 for SSPs based on the Padova tracks, but just [Z/H] ~ -2.2 for those based on the Frascati tracks). The differences are much smaller in the optical bands.

Also plotted are models by other EPS codes (Worthey 1994; Vazdekis et al. 1996, PEGASE.2, BC03 and Vázques & Leitherer 2005). All these models except those by Worthey (1994) adopt the stellar evolutionary tracks from the Padova data base and are computed by means of the isochrone synthesis technique. In spite of such harmony of model inputs, sizable discrepancies exist between these models. Interestingly, these type of discrepancies are larger than those induced by the use of different stellar tracks in our code. For example, the $V - K$ of the PEGASE.2 models with solar metallicity is nearly 0.2 mag. redder than that of the Vazdekis models, while BC03 agree with the latter in $V - I$ and with PEGASE.2 in $V - K$.

Note that in none of these other models the AGB phase transition is appreciable.

Also the metallicity scale shows quite a discrepancy, especially approaching large chemical abundances.

The scatter in the inferred ages and metallicities can be estimated directly from Fig. 27. We did not attempt a more quantitative evaluation since after all metallicities and ages should not be determined by means of one indicator, rather through a 'grid-like' approach.

As a final remark, the integrated colours of the Worthey (1994) models are typically redder than those of the other models. Charlot et al. (1996) attribute the effect to a factor of 2 more stars on the upper RGBs of G. Worthey isochrones than on the Padova isochrones used in the other two EPS. The fuel consumption approach helps to avoid such uncertainties.

---

[14] Note that our SSPs based on the Padova tracks do not include the TP-AGB phase, therefore the differences at $t \lesssim 2$ Gyr are not relevant in this context.
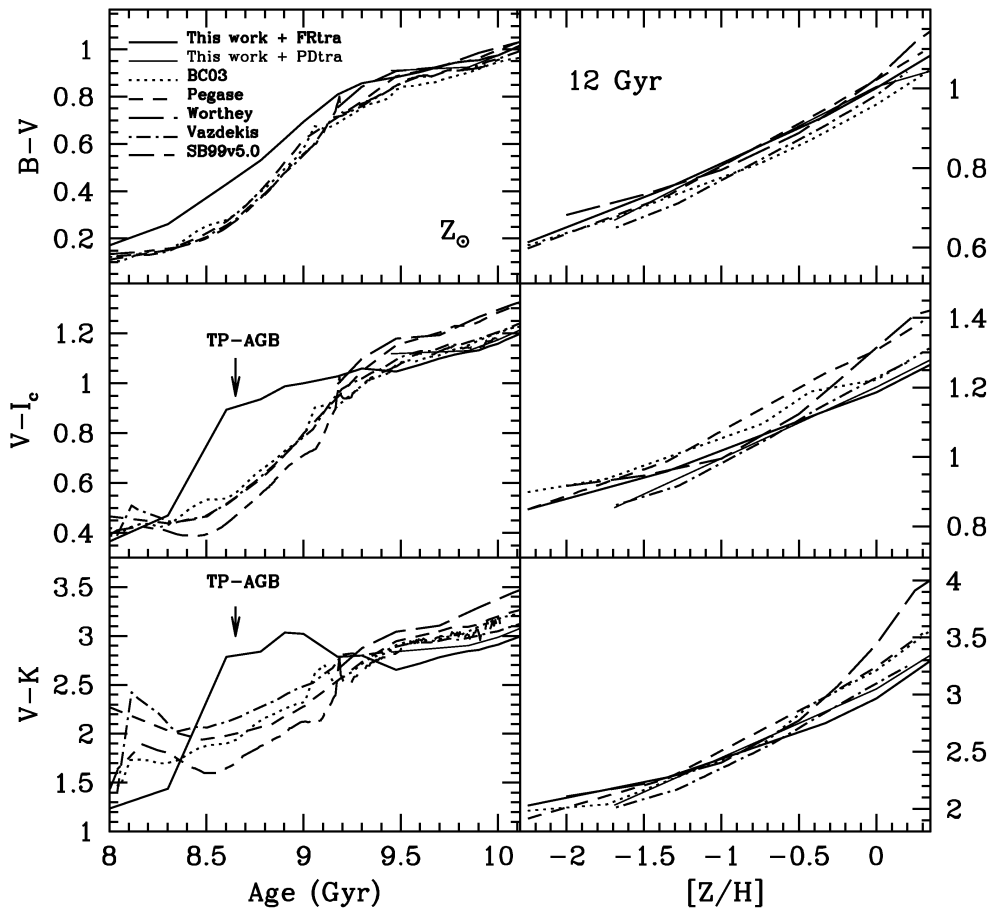
Figure 27. Effects of stellar models and EPS codes on colour–age (left-hand panel) and colour–metallicity at fixed age (12 Gyr) relations of stellar population models. The thin solid lines are SSP models computed with our code and the Padova stellar evolutionary tracks. The effect of the TP-AGB phase (see Sections 3.4.3 and 4 and Figs 18, 19 and 20) is highlighted.

6 A JUMP TO HIGH-z: TP-AGB STARS IN SPITZER GALAXIES?

As discussed in Section 3.1, the onset and development of the TP-AGB phase occupies a narrow age range in the evolutionary path of stellar populations, being confined to ages $0.3 \lesssim t \lesssim 2$ Gyr. During this short epoch the TP-AGB phase is the dominant one in a stellar population providing $\sim$40 per cent of the bolometric contribution, and up to $\sim$80 per cent of that in the K band (Fig. 13). Therefore, the inclusion of the TP-AGB phase in a stellar population model is essential for a correct interpretation of galaxies with stellar populations in this age range as discussed in Section 4.2.2 In particular, the TP-AGB phase can be used as an age indicator of intermediate-age stellar populations and its power is to be relatively robust against the age/metallicity degeneracy. In this direction goes the work by Silva & Bothun (1998), in which the two AGB-sensitive colours $J - H$ and $H - K$ were used to constrain the amount of intermediate-age stars in local, disturbed, field ellipticals. The authors rely on the comparison with colours of real TP-AGB stars after noticing that the population models they explored (Worthey 1994; Bruzual & Charlot 1993) neither reproduced the near-IR colours of local ellipticals nor were in agreement one with the other (the latter is confirmed by our comparison, see Fig. 27). Here we add that those models would not be suitable to the aim since they do not include the calibrated contribution by the TP-AGB phase (see

Section 4.2.2). The possible use of the TP-AGB as age indicator for high-z galaxies was first suggested by Renzini (1992).

At high redshifts when galaxies are dominated by $\sim$1 Gyr old populations as inferred from the ages and element ratios of local early-type galaxies (Thomas et al. 2005), the TP-AGB signature in the rest frame near-IR must show up, with e.g. the rest-frame $V - K$ colour mapping into the observed $K - 10$ μm at $z = 3$. This portion of the spectrum became recently available, thanks to the advent of the *Spitzer Space Telescope* (*SST*). Therefore, a straightforward application of the model SEDs presented in this paper is the interpretation of the high-z Spitzer galaxies as also discussed in Maraston (2004).

Recently Yan et al. (2004) published *SST*-IRAC data of galaxies in the *Hubble Ultra Deep* Field, with photometric redshifts ranging from 1.9 to 2.9. In order to explain the observed SEDs in the whole spectral range from the rest-frame B to K, in particular the high fluxes in both the blue and the near-IR, the authors must combine a dominant stellar population being at least 2.5 Gyr old, with traces (less than 1 per cent in mass) of a 0.1 Gyr old one. The relatively high age of the (dominant!) old component generally implies very high formation redshifts ($z_{\rm f} \gg 10$), and even exceeds the age of the Universe for the highest redshift objects.

This contrived solution is imposed by the evidence of very high observed fluxes in both the optical and near-IR rest frames. As we saw in Section 4.2.1 and Fig. 19, high near-IR fluxes in young stellar
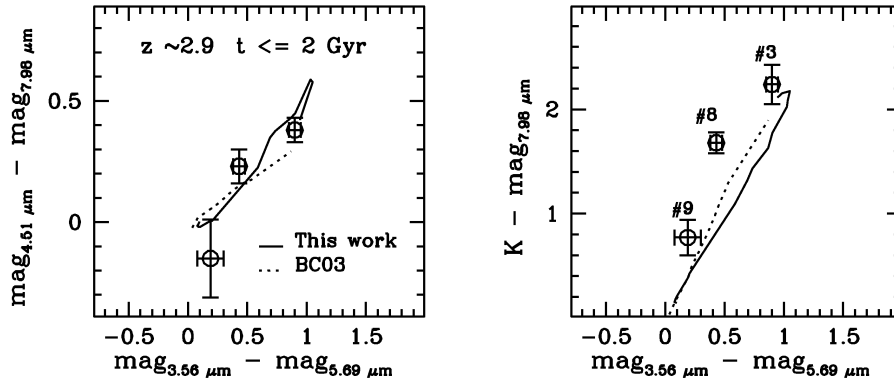
Figure 28. Two-colour diagrams in the IRAC (left-hand panel) and IRAC and K (right-hand panel) colours of the three highest-z objects (no. 3, no. 8, no. 9) of the Yan et al. (2004) sample. Magnitudes are in the AB system, and effective wavelengths of the IRAC filters are indicated. The y-axis of the right-hand panel corresponds to the rest-frame $V - K$. Dotted and solid lines refer to the models by BC03 (solar metallicity) and ours for 0.5 $Z_{\odot}$ plotted until the age of 2 Gyr, in order not to exceed the local age of the Universe (adopted cosmology $\Omega_M = 0.3$, $\Omega_\lambda = 0.7$, $H_0 = 73 \, \mathrm{km \, s^{-1} \, Mpc^{-1}}$).
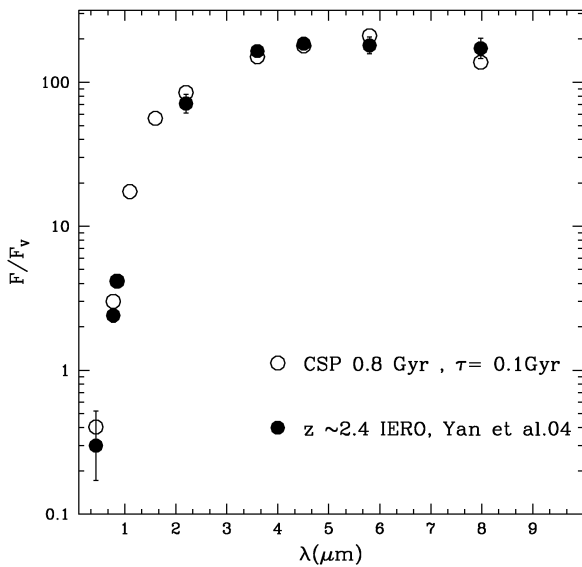

Figure 29. Comparison between the observed narrow-band fluxes of object no. 11 from Yan et al. (2004) and those of a 0.8-Gyr-old stellar population model with solar metallicity in which the stars are forming with an exponentially declining star formation rate with e-folding time of 0.1 Gyr.
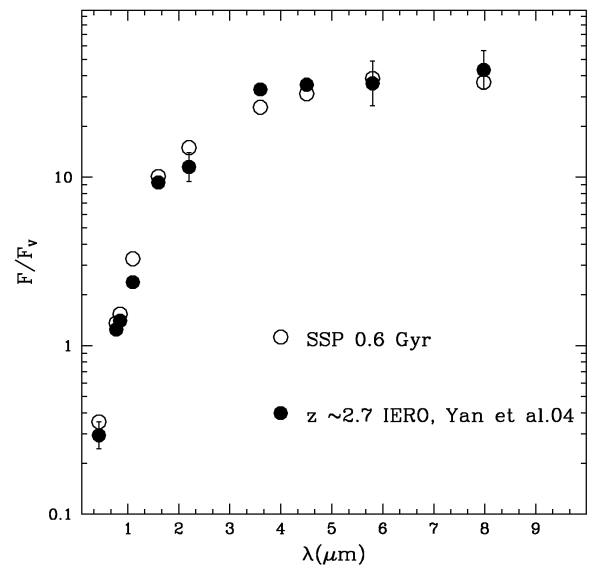

Figure 30. Comparison between the observed narrow-band fluxes of object no. 15 from Yan et al. (2004) and those of a 0.6 Gyr old metal-poor simple stellar population.

populations are the fingerprints of TP-AGB stars. It is therefore interesting to explore which ages are inferred from the models of this paper.

Fig. 28 shows two-colour diagrams in the IRAC+K observed frame, for the three highest-z objects of the Yan et al. (2004) sample. The y-axis in the right-hand panel corresponds to the rest-frame $V - K$, which is very sensitive to TP-AGB stars (cf. Fig. 20). At the nominal redshift of the objects ($z \sim 2.9$) the Universe is at most 2.3-Gyr-old in current cosmologies. The BC03 models (dotted lines) used by Yan et al. (2004) do not match the intrinsic $V - K$ of the reddest object (no. 3, right-hand panel) unless the age becomes 4 Gyr, which exceeds the age of the Universe. Our model (solid line) reaches the observed colours using ages around $\sim$1.5–2 Gyr instead. The inferred stellar mass for object no. 3 is $\sim 2.5 \times 10^{10} \, \mathrm{M_{\odot}}$. The other two objects in Fig. 28 look younger in these simple diagrams and seem to be in the pre-TP-AGB phase. However, object no. 8 has a rest-frame $V - K$ that is too red (or a rest-frame $I - J$ that is too

blue, x-axis) also for our standard models. A possible explanation could be reddening by dust, which would affect mostly the rest-frame V. Dust reddening was not found to be a promising solution by Yan et al. (2004), however, this might be also connected with their modelling lacking intrinsically red stars in the stellar population. A more detailed investigation is clearly beyond the scope of this paper and will be addressed in a subsequent work.

As a further example, Figs 29 and 30 show the fits to the whole SEDs for other two objects of the Yan et al. (2004) sample. In the first case the best 'by-eye' solution was found to be a composite stellar population (with solar metallicity) in which stars started to form 0.8 Gyr ago, with an exponentially declining star formation mode with e-folding time of 0.1 Gyr. In the second case, a single burst (i.e. an SSP) of 0.6 Gyr with low-metallicity ($Z_{\odot}/20$) was instead used. For both objects the whole SEDs are fitted reasonably well with lower ages, corresponding to formation redshifts of the order of $z \sim 3$. The derived stellar masses are $1.56 \times 10^{10} \, \mathrm{M_{\odot}}$ and $1.54 \times 10^9 \, \mathrm{M_{\odot}}$, respectively. Interestingly, in the latter case the mass and

the metallicity fit very well the corresponding relation obtained in the local Universe for dwarf early-type galaxies (Thomas et al. 2003b). This example opens the possibility that at least part of the very red galaxies could be objects caught during the full development of the TP-AGB phase.

The fits shown in Figs 29 and 30 are quite rudimentary and are meant to illustrate the application of the new models to high-z data. The 'best' solution was searched only 'by eye', without the help of statistical tools, which would go far beyond the scope of the paper. However, the match is encouraging and we will analyse more objects and in a more precise way in a future work.

7 SUMMARY

EPS models with various ages, metallicities, star formation histories and HB morphologies are presented. The evolutionary code is based on the fuel consumption theorem (RB86) for the evaluation of the energetics of the PMS evolutionary phases. The code was introduced in our previous work (M98) in which stellar population models were complete in all main stellar evolutionary phases, but were only computed for solar metallicity. The present paper provides the extension of the modelling to a wider range of stellar population parameters. The most important features of the models are: (i) the inclusion of the energetics and the spectra of TP-AGB stars and their calibrations with observations; and (ii) the allowance for various HB morphologies, in particular blue morphologies at high metallicities. We will come back to both points below.

In the first part of the paper we perform a comprehensive analysis of the model ingredients, focusing in particular on: (i) the metallicity effects on energetics and temperatures; (ii) the impact of different stellar evolutionary tracks. The most relevant results can be summarized as follows.

The energetics of stellar populations are higher at lower metallicity because of the greater hydrogen abundance. The most affected stellar phases are the MS and the helium-burning phase. The differences become smaller at ages later than the RGB phase-transition ($t \gtrsim 1$ Gyr) when the RGB phase becomes the most important contributor to the total bolometric. This is because the RGB fuel consumption is not affected dramatically by the chemical abundance, a result consistent with previous findings (Sweigart et al. 1989).

The impact of stellar evolutionary tracks is evaluated by comparing the energetics and temperatures of two different stellar models, namely the set of Frascati tracks by Cassisi and collaborators, which are classical tracks without overshooting, with those by the Padova school, which include the effects of overshooting. We find that the mass–luminosity relations for MS stars are rather similar among the explored tracks, which is explained by the modest amount of overshooting included in recent computations. Instead, major differences are found in post-MS phases, which involve both the energetics and the temperatures of the RGB. In the Padova tracks the onset and development of the RGB is delayed with respect to the Frascati tracks, an effect of overshooting. For example, a ∼0.8 Gyr stellar population model based on the Padova tracks has ∼30 per cent less light than one based on the Frascati tracks, a result influencing the integrated output, especially the M/L. It should be noticed that a recent comparison of the onset age of the RGB with what is observed in MC GCs favours the earlier RGB development of the Frascati tracks (Ferraro et al. 2004).

The temperatures of the RGB, especially towards the tip are cooler in the Padova tracks, at solar metallicity and above, a feature also found in the Yale tracks of Yi et al. (2003). The RGB temperature is the ingredient having the largest influence on the SSP output. For example, the integrated $V - K$ colours of old, metal-rich, stellar populations change by $\Delta V - K \sim 0.08$ mag. The RGB temperatures are connected to the mixing length and the underlying stellar models. The calibration of these effects is difficult since the comparisons with data require the adoption of temperature–colours transformations, that are uncertain as well. In spite of this, it would be highly valuable to understand the origin of such discrepancies at least theoretically.

Relevant to EPS models is the following result. The differences induced by the use of various stellar tracks in our code are substantially smaller than the scatter among stellar population models in the literature that adopt the same stellar tracks.

In the second part of the paper we describe in detail the recipes for the stellar phases that are affected by mass loss and therefore not described sufficiently by stellar evolutionary tracks. These are the HB in old stellar populations and the TP-AGB in stellar populations with ages between 0.2 and 2 Gyr. For the HB we apply mass loss to the RGB tracks such that we obtain a good match to stellar population spectrophotometric indicators that are sensitive to the HB morphology (e.g. the Balmer lines). We therefore calibrate the amount of mass loss with MW GCs of known HB morphology. In order to account for the observed scatter in the HB properties at a fixed metallicity, we provide the models with a couple of choices for the HB morphology. In particular, we also compute blue HB at high Z and show how much blue indicators like e.g. the Balmer lines and the U, B, V magnitudes are affected. The effects of BHBs at high Z are quantified in a form that can be easily used also when other EPS are adopted.

A result interesting for extragalactic GC studies is that the D-4000 Å break, unlike the Balmer lines is insensitive not only to age but also to the HB morphology at low metallicity ([Z/H] $\lesssim$ −1). Therefore, this colour can be used as metallicity indicator in the metal-poor regime.

The energetic of the TP-AGB phase was calibrated with Magellanic Cloud GCs data in (M98). It was shown that this phase is the dominant one in stellar populations with ages between 0.3 and 2 Gyr, providing 40 per cent of the bolometric and up to 80 per cent of the luminosity in the near-IR. Here we make a step forward by including the spectra of TP-AGB stars in the synthetic SEDs of the stellar population models, using available empirical spectra of TP-AGB C-rich and O-rich stars. We compare the resulting model SEDs with the observed SEDs of a sample of MC GCs with data from U to K. The models provide a very good fit to the data in the whole age range relevant to the TP-AGB, a success that is entirely due to the proper inclusion of the phase in the models. We further compute the integrated spectral indices C_2, H_2O and CO in the near-IR (1.7 $\lesssim \lambda/\mu m \lesssim$ 2.4), which are effective tracers of C and O stars. We find that the combination of C_2 and H_2O can be used to determine the metallicity of ∼1-Gyr-stellar populations, independently of the star formation history.

The model SEDs presented here can be applied to the analysis of high-z galaxies extending the concept of TP-AGB as age indicator for ∼1-Gyr stellar populations to primeval objects in the early Universe. As an illustrative application we re-analyse some high-z (2.4 $\lesssim z \lesssim$ 2.9) galaxies recently observed with the *SST* (Yan et al. 2004). The distinctive feature of these objects is to have strong fluxes in both the rest frames – blue and near-IR – relative to the flux in the V band. This is what characterizes TP-AGB-dominated stellar populations. We show that the data can be explained by stellar populations with ages in the range 0.6–1.5 Gyr. These ages are comfortable given the age of the Universe at those redshifts (∼2 Gyr) and imply formation redshifts between 3 and 6.

Models are available at www-astro.physics.ox.ac.uk/~maraston.

REFERENCES

Aaronson M., Frogel J. A., Persson S. E., 1978, ApJ, 220, 442
Alvarez R., Lançon A., Plez B., Plez B., Wood P. R., 2000, A&A, 353, 322
Armandroff T. E., Zinn R., 1988, AJ, 96, 92
Arimoto N., Yoshii Y., 1986, A&A, 164, 260
Barbaro G., Pigatto L., 1984, A&A, 136, 335
Barbaro G., Poggianti B. M., 1997, A&A, 324, 490
Ballik E. A., Ramsay D. A., 1963, ApJ, 137, 61
Barbuy B., Renzini A., Ortolani S., Bica E., Guarnieri M. D., 1999, A&A, 341, 539
Barmby P., Huchra J. P., 2000, AJ, 119, 727
Bertelli G., Nasi E., Girardi L., Chiosi C., Zoccali E., Gallart C., 2003, AJ, 125, 770
Bergbusch P. A., VandenBerg D. A., 1992, ApJS, 81, 163
Bergbusch P. A., VandenBerg D. A., 2001, ApJ, 556, 322
Bessel M. S., Brett J. M., Wood P. R., Scholz M. et al., 1989, A&AS, 77, 1
Block D. L., Freeman K. C., Jarrett T. H., Puerari I., Worthey G., Combes F., Groess R., 2004, A&A, 425, L37
Bloecker T., Schoenberner D., 1991, A&A, 244, L43
Bono G., Caputo F., Cassisi S., Castellani V., Marconi M., 1997, ApJ, 489, 822
Boothroyd A. I., Sackmann I. J., 1988, ApJ, 328, 632
Bressan A., Granato G. L., Silva L., 1998, A&A, 332, 135
Brocato E., Castellani V., Poli F. M., Raimondo G., 2000, A&AS, 146, 91
Bruzual G. A., 1983, ApJ, 273, 105
Bruzual G. A., Charlot S., 1993, ApJ, 405, 538
Bruzual G. A., Charlot S., 2003, MNRAS, 344, 1000
Buzzoni A., 1989, ApJS, 71, 817
Cassisi S., Salaris M., 1997, MNRAS, 285, 593
Cassisi S., Castellani M., Castellani V., 1997a, A&A, 317, 108
Cassisi S., Degl'Innocenti S., Salaris M., 1997b, MNRAS, 290, 515
Cassisi S., Castellani V., Ciarcielluti P., Piotto G., Zoccali M., 2000, MNRAS, 315, 679
Castellani V., Chieffi A., Straniero O., 1992, ApJS, 78, 517
Cenarro A. J., Cardiel N., Gorgas J., Peletier R. F., Vazdekis A., Prada F., 2001a, MNRAS, 326, 959
Cenarro A. J., Gorgas J., Cardiel N., Pedraz S., Peletier R. F., Vazdekis A., 2001b, MNRAS, 326, 981
Cenarro A. J., Gorgas J., Cardiel N., Vazdekis A., Peletier R. F., 2002, MNRAS, 329, 863
Charlot S., Bruzual G., 1991, ApJ, 367, 126
Charlot S., Worthey G., Bressan A., 1996, ApJ, 457, 625
Chiosi C., Bertelli G., Bressan A., 1988, A&A, 196, 84
Cohen J. G., Carretta E., Gratton R. G., Behr B. B., 1999, AJ, 122, 1469
Davidge T. J., 2003, ApJ, 597, 289
de Freitas Pacheco J. A., Barbuy B., 1995, A&A, 302, 718
De Santi R., Cassisi S., 1999, MNRAS, 308, 9
Diaz A. I., Terlevich E., Terlevich R., 1989, MNRAS, 239, 325
Dickens R. J., 1972, MNRAS, 157, 281
Faber S. M., 1972, A&A, 20, 361

Fagotto F., Bressan A., Bertelli G., Chiosi C., 1994, A&AS, 105, 29
Ferraro F., Fusi Pecci F., Testa V., Greggio L., Corsi C. E., Buonanno R., Terndrup D. M., Zinnecker H., 1995, MNRAS, 272, 391
Ferraro F., Origlia L., Testa V., Maraston C., 2004, ApJ, 608, 772
Fioc M., Rocca-Volmerange B., 1997, A&A, 326, 950
Frogel J. A., Persson S. E., Matthews K., Aaronson M., 1978, ApJ, 220, 75
Frogel J. A., Mould J. R., Blanco V. M., 1990, ApJ, 352, 96
Fusi Pecci F., Renzini A., 1976, A&A, 46, 447
Girardi L., Chiosi C., Bertelli G., Bressan A., 1995, A&A, 298, 87
Girardi L., Bressan A., Bertelli G., Chiosi C., 2000, A&AS, 141, 371
Gorgas J., Cardiel N., Pedras S., Gonzales J. J., 1999, A&AS, 139, 29
Greggio L., 1997, MNRAS, 301, 166
Greggio L., Renzini A., 1990, ApJ, 364, 35
Gronewegen M. A. T., de Jong T., 1993, A&A, 267, 410
Harris W. E., 1996, AJ, 112, 1487
Iben I., Jr, Renzini A., 1983, ARA&A, 21, 271
Kim Y.-C., Demarque P., Yi S. K., Alexander D. R., 2002, ApJS, 143, 499
Kodama T., Arimoto N., 1997, A&A, 320, 41
Kroupa P., 2001, MNRAS, 322, 231
Kurucz R. L., 1979, ApJS, 40, 1
Lançon A., Mouhcine M., 2002, A&A, 393, 167
Lançon A., Wood P. R., 2000, A&AS, 146, 217
Lançon A., Mouhcine M., Fioc M., Silva D., 1999, A&A, 344, L21
Lattanzio J. C., 1986, ApJ, 311, 708
Le Borgne J. F. et al., 2003, A&A, 402, 433
Le Borgne D., Rocca-Volmerange B., Prugniel P., Lançon A., Fioc M., Soubiran C., 2004, A&A, 425, 881
Lee H., Yoon S. J., Lee Y. W., 2000, AJ, 120, 998
Leitherer C. et al., 1999, ApJS, 123, 40
Lejeune T., Cuisinier F., Buser R., 1998, A&AS, 130, 65
Lloidl R., Lançon A., Jorgensen U. G., 2001, A&A, 371, 1065
Maraston C., 1998, MNRAS, 300, 872
Maraston C., 2004, in Renzini A., Bender R., eds, Proc. II Venice Conf., Multiwavelength Mapping of Galaxy Evolution.
Maraston C., Thomas D., 2000, ApJ, 541, 126
Maraston C., Kissler-Patig M., Brodie J., Barmby P., Huchra J. P., 2001a, A&A, 370, 176
Maraston C., Greggio L., Thomas D., 2001b, Ap&SS, 276, 893
Maraston C., Greggio L., Renzini A., Ortolani S., Saglia R. P., Puzia T. H., Kissler-Patig M., 2003, A&A, 400, 823
Maraston C., Bastian N., Saglia R. P., Kissler-Patig M., Schweizer F., Goudfrooij P., 2004, A&A, 416, 467
Marigo P., 2001, A&A, 370, 194
Marigo P., Bressan A., Chiosi C., 1996, A&A, 313, 545
Marigo P., Bressan A., Chiosi C., 1999, A&A, 344, 123
Matteucci F., 1994, A&A, 288, 57
Meynet G., Maeder A., Schaller G., Schaerer D., Charbonnel C., 1994, A&AS, 103, 97
Michaud G., Richard O., Richer J., VandenBerg D. A., 2004, ApJ, 606, 452
Miller B. W., Whitmore B. C., Schweizer F., Fall S. M., 1997, AJ, 114, 2381
Mollà M., Garcia-Vargas M. L., 2000, A&A, 359, 18
Mouhcine M., Lançon A., 2002, A&A, 393, 149
Mouhcine M., Lançon A., Leitherer C., Silva D., Gronewegen M. A. T., 2002, A&A, 393, 101
O'Connell R. W., 1980, ApJ, 236, 430
Ortolani S., Renzini A., Gilmozzi R., Marconi G., Barbuy B., Bica E., Rich M., 1995, Nat, 377, 701
Persson S. E., Aaronson M., Cohen J. G., Frogel J. A., Matthews K., 1983, ApJ, 266, 105
Piotto G. et al., 2002, A&A, 391, 945
Reimers D., 1977, A&A, 61, 217
Renzini A., 1981, in Silk J., Vittorio J., eds, Galaxy Formation. Amsterdam, North Holland, p. 303
Renzini A., 1992, in Barbuy B., Renzini A., eds, IAU Symp., 149, The Stellar Populations of Galaxies. Kluwer, Dordrecht, p. 325
Renzini A., Buzzoni A., 1986, in Chiosi C., Renzini A., eds, Spectral Evolution of Galaxies. Dordecht, Reidel, p. 195
Renzini A., Ciotti L., 1993, ApJ, 416, L49

Renzini A., Fusi Pecci F., 1988, ARA&A, 26, 199
Renzini A., Voli M., 1981, A&A, 94, 175
Rich M. et al., 1997, ApJ, 484, L25
Rocca-Volmerange B., Guiderdoni B., 1987, A&A, 175, 15
Rosenberg A., Saviane I., Piotto G., Aparicio A., 1999, AJ, 118, 2306
Saglia R. P., Maraston C., Greggio L., Bender R., Ziegler B., 2000, A&A, 360, 91
Saglia R. P., Maraston C., Thomas D., Bender R., Colless M., 2002, ApJL, 444, 111
Salaris M., Cassisi S., 1996, A&A, 305, 858
Salasnich B., Girardi L., Weiss A., Chiosi C., 2000, A&A, 361, 1023
Salpeter E. E., 1955, ApJ, 121, 161
Schaller G., Schaerer D., Meynet G., Maeder A., 1992, A&AS, 96, 269
Schlegel D. A., Finkbeiner D. P., Davis M., 1998, ApJ, 500, 525
Schiavon R. P., Barbuy B., Bruzual G., 2000, ApJ, 532, 453
Schweizer F., Seitzer P., 1998, AJ, 116, 2206
Searle L., Wilkinson A., Bagnuolo W. G., 1980, ApJ, 239, 803
Silva D. R., Bothun G. D., 1998, ApJ, 116, 85
Sweigart A. V., Greggio L., Renzini A., 1989, ApJS, 69, 911
Sweigart A. V., Greggio L., Renzini A., 1990, ApJ, 364, 527
Tantalo R., Chiosi C., Bressan A., Fagotto F., 1996, A&A, 311, 361
Tinsley B. M., 1972, A&A, 20, 383
Tinsley B. M., Gunn J. E., 1976, ApJ, 203, 52
Thomas D., Maraston C., 2003, A&A, 311, 361
Thomas D., Greggio L., Bender R., 1999, MNRAS, 302, 537
Thomas D., Maraston C., Bender R., 2003a, MNRAS, 311, 361

Thomas D., Bender R., Hopp U., Maraston C., Greggio L., 2003b, Ap&SS, 284, 599
Thomas D., Maraston C., Korn A., 2004, MNRAS, 351, L19
Thomas D., Maraston C., Bender R., Mendes de Oliveira C., 2005, ApJ, 621, 673
Tinsley B. M., 1980, ApJ, 241, 41
VandenBerg D. A., Clem J. L., 2003, AJ, 126, 802
van den Bergh S., 1981, A&AS, 46, 79
Vassiliadis E., Wood P. R., 1993, 413, 641
Vazdekis A., Casuso E., Peletier R. F., Beckmann J. E., 1996, ApJS, 103, 307
Vazdekis A., Cenarro A. J., Gorgas J., Cardiel N., Peletier R. F., 2003, MNRAS, 340, 1317
Vázques G. A., Leitherer C., 2005, ApJ, 621, 717
Wagenhuber J., Groenewegen M. A. T., 1998, A&A, 340, 183
Woo J.-H., Gallart C., Demarque P., Yi S., Zoccali M., 2003, AJ, 125, 754
Worthey G., 1994, ApJS, 95, 107
Worthey G., Ottaviani D. L., 1997, ApJS, 111, 377
Worthey G., Faber S. M., González J. J., Burstein D., 1994, ApJS, 94, 687
Yan H. et al., 2004, ApJ, 616, 63
Yi S. K., Kim, Y.-C., Demarque P., 2003, ApJS, 144, 259
Zinn R., West M. J., 1984, ApJS, 55, 45

This paper has been typeset from a TEX/LATEX file prepared by the author.